Molecular Neurodegeneration

RESEARCH ARTICLE

Open Access

Border-associated macrophages promote cerebral amyloid angiopathy and cognitive impairment through vascular oxidative stress

Ken Uekawa[1], Yorito Hattori[1], Sung Ji Ahn[1], James Seo[1], Nicole Casey[1], Antoine Anfray[1], Ping Zhou[1], Wenjie Luo[1], Josef Anrather[1], Laibaik Park[1*] and Costantino Iadecola[1*]

Abstract

Background Cerebral amyloid angiopathy (CAA) is a devastating condition common in patients with Alzheimer's disease but also observed in the general population. Vascular oxidative stress and neurovascular dysfunction have been implicated in CAA but the cellular source of reactive oxygen species (ROS) and related signaling mechanisms remain unclear. We tested the hypothesis that brain border-associated macrophages (BAM), yolk sac-derived myeloid cells closely apposed to parenchymal and leptomeningeal blood vessels, are the source of radicals through the Aβ-binding innate immunity receptor CD36, leading to neurovascular dysfunction, CAA, and cognitive impairment.

Methods Tg2576 mice and WT littermates were transplanted with $CD36^{-/-}$ or $CD36^{+/+}$ bone marrow at 12-month of age and tested at 15 months. This approach enables the repopulation of perivascular and leptomeningeal compartments with $CD36^{-/-}$ BAM. Neurovascular function was tested in anesthetized mice equipped with a cranial window in which cerebral blood flow was monitored by laser-Doppler flowmetry. Amyloid pathology and cognitive function were also examined.

Results The increase in blood flow evoked by whisker stimulation (functional hyperemia) or by endothelial and smooth muscle vasoactivity was markedly attenuated in WT → Tg2576 chimeras but was fully restored in $CD36^{-/-}$ → Tg2576 chimeras, in which BAM ROS production was suppressed. CAA-associated $A\beta_{1\text{-}40}$, but not $A\beta_{1\text{-}42}$, was reduced in $CD36^{-/-}$ → Tg2576 chimeras. Similarly, CAA, but not parenchymal plaques, was reduced in $CD36^{-/-}$ → Tg2576 chimeras. These beneficial vascular effects were associated with cognitive improvement. Finally, $CD36^{-/-}$ mice were able to more efficiently clear exogenous $A\beta_{1\text{-}40}$ injected into the neocortex or the striatum.

Conclusions CD36 deletion in BAM suppresses ROS production and rescues the neurovascular dysfunction and damage induced by Aβ. CD36 deletion in BAM also reduced brain $A\beta_{1\text{-}40}$ and ameliorated CAA without affecting parenchyma plaques. Lack of CD36 enhanced the vascular clearance of exogenous Aβ. Restoration of neurovascular function and attenuation of CAA resulted in a near complete rescue of cognitive function. Collectively, these data implicate brain BAM in the pathogenesis of CAA and raise the possibility that targeting BAM CD36 is beneficial in CAA and other conditions associated with vascular Aβ deposition and damage.

Keywords Border-associated macrophages, CD36, Aβ clearance, Neurovascular unit dysfunction, Vascular oxidative stress, ARIA

*Correspondence:
Laibaik Park
lap2003@med.cornell.edu
Costantino Iadecola
coi2001@med.cornell.edu
Full list of author information is available at the end of the article

Graphical Abstract

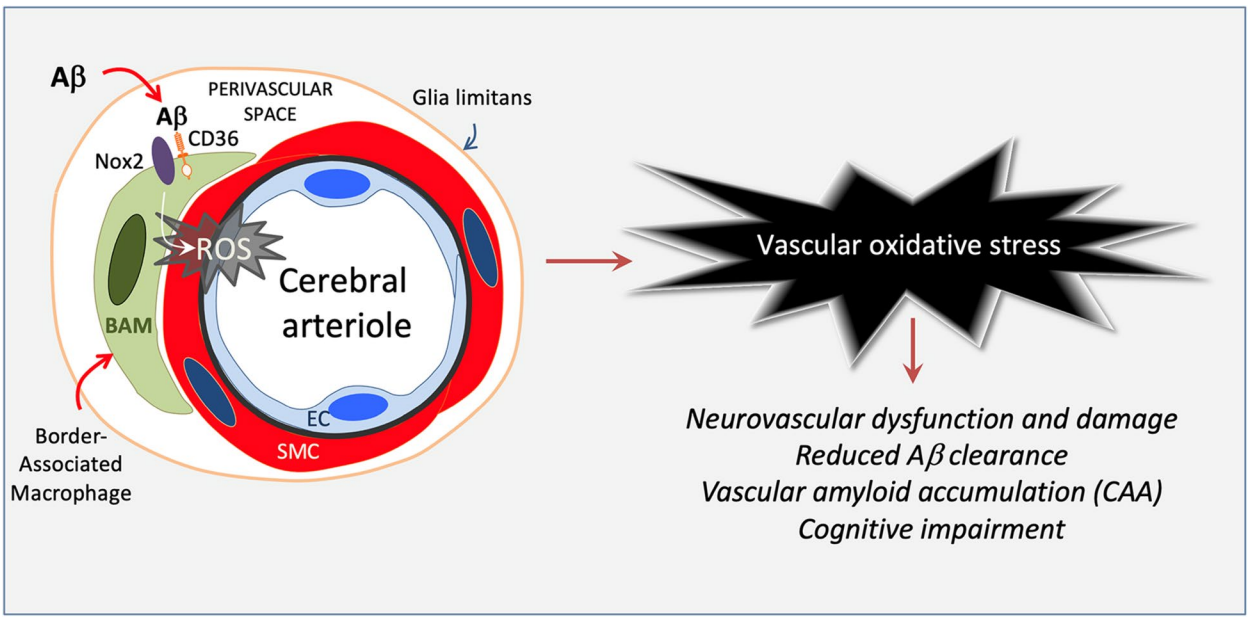

Background

Deposition of amyloid-β (Aβ) in cerebral blood vessels (cerebral amyloid angiopathy; CAA) is a key pathological feature of Alzheimer's disease (AD) [1]. CAA also occurs independently of AD and can either be sporadic or caused by mutations of the amyloid precursor protein (APP) [2]. Amyloid deposition is observed first in the wall of cerebral arterioles wherein the short form of Aβ ($Aβ_{1-40}$) is the prevalent peptide that accumulates [3–5]. CAA has devastating consequences for brain health leading to parenchymal hemorrhages, microbleeds, white matter lesions, and superficial cortical siderosis, and, to date, remains untreatable [2].

Increasing evidence implicates failure of vascular Aβ clearance in the mechanisms of CAA [2, 6]. Aβ is released in the extracellular space during neural activity and is promptly removed by various mechanisms, including vascular clearance [6]. Once in the perivascular space, Aβ is transported across the vessel wall into the blood [7–9] or conveyed from the perivascular space to the subarachnoid space where it reaches the CSF [10–13]. From the subarachnoid space Aβ is transported out of the brain via CSF clearance pathways through venous and lymphatic vessels [11, 14].

Cerebrovascular health is essential for the vascular clearance of Aβ and alterations in neurovascular function have been implicated in CAA [2]. Suppression of the ability of neural activity to increase cerebral blood flow (CBF) (functional hyperemia), a fundamental homeostatic response of the cerebral microcirculation [15], occurs early in patients with CAA [16–18], whereas Aβ-induced suppression of functional hyperemia and dysfunction of the endothelial regulation of CBF have been linked to CAA in mouse models [13, 19–21]. Aβ-induced vascular oxidative stress and the attendant neurovascular dysregulation and damage have emerged as key factors in CAA both in mouse models [19, 20] and in humans [22]. However, the cellular sources of the reactive oxygen species (ROS) and the related signaling mechanisms remain to be established.

Brain border-associated macrophages (BAM), like microglia, are yolk sack-derived myeloid cells that reach the brain and populate meninges, perivascular spaces, and choroid plexus [23]. In particular, BAM in leptomeningeal and perivascular spaces are closely associated with cerebral blood vessels and a major source of vascular oxidative stress through the ROS-producing enzyme Nox2 [24–26]. The Aβ-binding scavenger receptor CD36 has been linked to AD [27, 28] and is upregulated in CAA [29]. CD36 is enriched in BAM and underlies the oxidative stress and neurovascular dysfunction induced by Aβ [30, 31]. In pre-symptomatic (age 3 months) transgenic mice expressing the Swedish mutation of APP (Tg2576), Aβ triggers vascular oxidative stress by activating CD36 in BAM, which, in turn, mediates the attendant suppression of functional hyperemia and endothelial vasoactive

function [25]. However, it remains to be established if BAM are responsible for the vascular accumulation of Aβ in older Tg2576 mice with florid amyloid pathology and cognitive impairment. Therefore, in this study we used a bone marrow (BM) chimera-based approach to investigate the role of BAM in the neurovascular dysfunction, cognitive impairment, vascular pathology and CAA in 15-month-old Tg2576 mice.

Materials and methods

Mice

The Institutional Animal Care and Use Committee of Weill Cornell Medicine approved all experimental procedures. Experiments were performed in 12–15 month-old transgenic mice overexpressing the Swedish mutation of the amyloid precursor protein (APP) (Tg2576) [32] or age-matched WT littermates, referred to as WT mice. In bone marrow (BM) chimera experiments, WT and $CD36^{-/-}$ mice were used as BM donors. Some studies used GFP^{+} mice (JAX Stock #006567) as BM donors. All mice were males and derived from in-house colonies [25, 30, 31, 33, 34].

Bone marrow transplantation

Procedures for BM transplantation have been previously described [24, 25, 35] and are only summarized. Whole-body irradiation was performed in 12-month-old mice with a lethal dose of 9.5 Gy of γ radiation using a 137Cs source (Nordion Gammacell 40 Exactor). Eighteen hours later, mice were transplanted with BM cells (2×10^6, i.v.) isolated from $CD36^{-/-}$ and WT controls. Mice were housed in cages with sulfamethoxazole (0.12%; w/v) and trimethoprim (0.024%) added to drinking water for the first two weeks. Reconstitution of BM cells was verified five weeks after irradiation by testing the positive CD36 genomic DNA percentage in isolated blood leukocytes [35]. Reference primers sequences were as follows: m_ICAM1_prom.3, 5′-GGACTCACCTGCTGGTCT CT-3′ and m_ICAM1_prom.4, 5′-GAACGAGGGCTT CGGTATTT-3′; target primers sequences were as follows: CD36_1, 5'- -3' and CD36_2, 5'- -3', m_Cybb_gt_1, 5'-CTGCTCACCAGCCTCTCTCTA-3' and m_Cybb_gt_2, 5'-CTGGAACCCCTGAGAAAGGAG-3' (Invitrogen). qRT-PCR was conducted with 20 ng of DNA, in duplicate 15 µl reactions using the Maxima SYBR Green/ROX qPCR Master Mix (2×) (Thermo Scientific). Chimerism was > 95% for $CD36^{-/-}$ BM chimeras. A PCR cycling protocol consisting of 15 s at 95°C and 1 min at 60°C for 45 cycles was used for quantification CD36 relative expression levels were calculated by the 2 (−ΔΔ CT) method. To study BAM number and distribution after BM transplant in Tg2576 mice, BM from mice expressing GFP (GFP BM) was transplanted into Tg2576 mice or WT littermates at 3 or 12 months of age and the brain distribution of GFP expressing cells was examined at 15 months of age. In some experiments, GFP BM was transplanted into irradiated WT mice with head shielding at 3 months and GFP-expressing cells were examined 3 months later.

CBF measurement

Surgical procedures

As described in detail elsewhere [30, 31, 33, 34], mice were anesthetized with isoflurane (induction, 5%; surgery, 1.5%) and maintained with urethane (750 mg/kg; i.p.) and α-chloralose (50 mg/kg; i.p.). A femoral artery was cannulated to record arterial pressure and collect blood samples for blood gas analysis. The trachea was intubated and mice were artificially ventilated with a mixture of N_2 and O_2. Arterial blood pressure (80–90 mmHg), blood gases (pO_2, 120–140 mmHg; pCO_2, 30–40 mmHg; pH, 7.3–7.4), and rectal temperature (37 °C) were monitored and controlled. Throughout the experiment, the level of anesthesia was monitored by testing motor responses to tail pinch. The somatosensory cortex was exposed through a small craniotomy (2×2 mm). The dura was removed, and the exposed cortex was continuously bathed with a modified Ringer's solution (36–37 °C; pH: 7.3–7.4) (see ref. [36] for composition). CBF was continuously monitored at the site of superfusion with a laser-Doppler probe (Vasamedic, St. Paul, MN) positioned stereotaxically on the neocortical surface and connected to a computerized data acquisition system. CBF values were expressed as a percent increase relative to the resting level. Resting CBF is reported as arbitrary laser-Doppler perfusion units (LDU). Zero values for CBF were obtained after stopping the heart at the end of the experiment.

Experimental protocol

CBF recordings were started after arterial pressure and blood gases were stable. To test functional hyperemia, the CBF response evoked by gently stroking the whiskers with a cotton-tipped applicator for 60 s was recorded. To test endothelium-dependent vasodilatation, acetylcholine (10 µM, Sigma), the Ca^{2+} ionophore A23187 (3 µM; Sigma) or bradykinin (50 µM; Sigma) was topically superfused for 3–5 min and the evoked CBF increases recorded. To test smooth muscle function, the CBF responses to adenosine (400 µM, Sigma) or to the NO donor S-Nitroso-N-acetyl-DL-penicillamine (SNAP; 50 µM, Sigma) were examined [25, 31, 37]. All pharmacological agents were dissolved in a modified Ringer's solution [36]. The increase in CBF produced by hypercapnia was tested by introducing 5% CO_2 in the ventilator to increase arterial pCO_2 up to 50–60 mmHg. Once a stable

increase in CBF was obtained for 3–5 min, pCO_2 was returned to normocapnia.

Intracerebroventricular injection of dextran

BAM were identified by their ability to phagocytize dextran [24, 25, 38]. For dextran injections, 10 µl of Alexa Fluor® 680 dextran (10,000 MW, anionic, fixable, ThermoFisher Scientific, D34680; 2.5 mg/ml) in saline or saline alone were slowly injected into the cerebral ventricles with a glass micropipette through a burr hole drilled on the right parietal bone [25]. BAM labeling was examined 24 h later.

Labeling cortical blood vessels with DiO

Cortical blood vessels were labeled with the lipophilic dye DiO [DiOC18(3) (3,3'-Dioctadecyloxacarbocyanine Perchlorate)], as described [25, 39]. Briefly, mice were anesthetized (5% isoflurane) and transcardially perfused with PBS (2 ml) followed by DiO (1:50, V-22886, Molecular Probes; 5 ml/mouse) and then by 4% paraformaldehyde (PFA). Brains were harvested and post-fixed in 4% PFA overnight, then cut (thickness 150 µm) using a vibratome and examined under the confocal microscope (Leica SP8).

Immunohistochemistry

Mice were anesthetized with sodium pentobarbital (120 mg/kg, i.p.) and perfused transcardially with PBS followed by 4% PFA in PBS. Brains were removed, post-fixed overnight, and sectioned coronally in a vibratome (section thickness: 40 µm). In some experiments, cortices were dissected out, flattened and post-fixed overnight. The cortices were tangentially sectioned as above. Free-floating brain sections were permeabilized with 0.5% Triton X-100 and non-specific binding was blocked with 1% of normal donkey serum. Sections were randomly selected and incubated with the primary antibodies CD206 (clone MR5D3, rat polyclonal, 1:200, Serotec), CD36 (mouse monoclonal, 1:500, BD Biosciences), Glut-1 (rabbit polyclonal, 1:200, Calbiochem), Iba-1 (rabbit polyclonal, 1:500, Wako Chemicals), α-Actin (rabbit polyclonal, 1:300, abcam), or GFAP (mouse monoclonal, 1:1000, Sigma) overnight at 4°C. After washing, brain sections were incubated with a Cy5- or a FITC-conjugated secondary antibody (1:200; Jackson ImmunoResearch Laboratories), mounted on slides and imaged with a confocal microscope (Leica SP8). In some experiments, brain sections were con-stained with thioflavin-S (0.5%) to assess amyloid plaques and CAA. The specificity of the immunofluorescence was verified by the omission of the primary and/or secondary antibody or blocking the antigen. All quantifications were performed by investigators blinded to the treatment on randomly selected fields within the somatosensory cortex.

Identification and quantification of BAM in the somatosensory cortex

BAM were identified by well-established criteria, including expression of CD206, ability to phagocytize dextran and perivascular location [24, 25, 40, 41]. The association with cortical blood vessels was confirmed by co-labeling with the endothelial marker Glut-1 (rabbit polyclonal, 1:200, Calbiochem), α-Actin (rabbit polyclonal, 1:300, abcam), or DiO [25, 39]. For $CD206^+$ BAM, randomly selected fields (20× objective; 4 confocal images/mouse; $n=5$ mice/group) within the somatosensory cortex were analyzed. For $dextran^+$ BAM, a representative coronal section from each mouse was reconstructed from tiled images taken with the confocal microscope, and the whole somatosensory cortex ($n=5$/group) was analyzed. ImageJ (NIH) was used for all image analyses.

ROS measurement

ROS production was assessed in vivo by dihydroethidine (DHE) microfluorography [24, 25, 30, 42, 43]. BM-transplanted WT or Tg2576 mice were first injected with icv dextran (see above). The day after the dextran injection, DHE (10 mg/kg; Invitrogen) was infused into the jugular vein in mice under isoflurane anesthesia. Sixty minutes after DHE administration, mice were transcardially perfused with DiO to label cerebral blood vessels as described above and before [25, 39]. Coronal brain sections were then cut through the cortex underlying the cranial window, and ROS-dependent fluorescence associated with BAM was quantified as described previously [24, 25, 42].

Brain Aβ measurement

Brain Aβ was measured using an ELISA-based assay as described previously [34]. Briefly, the left hemispheres of the mice used for CBF studies were homogenized with RIPA followed by a 5.5 M guanidine buffer containing a cocktail of protease inhibitors (1:1000; Roche). Aβ measured after the RIPA extraction represented the soluble pool of Aβ, whereas Aβ measured after guanidine extraction represented the insoluble pool. The homogenates were diluted with a cold sample dilution buffer (1% bovine serum albumin in PBS and 0.05% Tween 20 [PBST]) before measurement of $Aβ_{1–40}$ or $Aβ_{1–42}$. Guanidine-solubilized samples were diluted with a cold sample dilution buffer to a final concentration of 0.5 M GuHCl. Samples were loaded onto plates coated with an antibody that specifically recognizes the C-terminal domain of $Aβ_{1–42}$ (21F12) or $Aβ_{1–40}$ (2G3) as the capture antibody, and biotinylated 3D6 was used for detection. The

immunoreactivity signal after incubation with horseradish peroxidase-conjugated streptavidin (Research Diagnostics) was developed with a TMB substrate (Thermo Fisher Scientific) and read on a Synergy H1 Hybrid plate reader (BioTek). Levels of Aβ were calculated using a standard curve generated with recombinant human Aβ (American Peptide Company). Levels of Aβ in brain homogenates were determined in triplicate, normalized to protein content, and expressed as the amount of Aβ per milligram of protein. Concentrations in picomoles per milligram of brain tissue were calculated by comparing the sample absorbance with the absorbance of known concentrations of synthetic $A\beta_{1-40}$ and $A\beta_{1-42}$.

Amyloid burden, CAA and smooth muscle cell fragmentation

In vivo CAA imaging

We imaged pial vessel CAA using 2-photon microscopy. Optical access to the brain was achieved through a polished and reinforced thinned skull preparation sealed with cyanoacrylate glue and a cover glass [26, 33]. Mice were allowed at least two weeks to recover from window implantation. To label Aβ deposits, methoxy-X04 (Tocris, dissolved in DMSO at 100 mM) was intraperitoneally injected one day before imaging at a dose of 1 mg/100 g [44]. To fluorescently label the blood vessel, Texas Red dextran (40 µl, 2.5%, molecular weight (MW) = 70,000 kDa, Thermo Fisher Scientific) in saline was injected retro-orbitally immediately before imaging. Imaging was performed on a commercial 2-photon microscope (FVMPE; Olympus) with XLPlan N 25 × 1.05 NA objective. Excitation pulses came from a solid-state laser (InSight DS+; Spectraphysics) set at 830 nm wavelength. Image stacks were acquired through Fluoview software. During imaging, anesthesia was maintained with ~ 1.5% isoflurane in an oxygen/nitrogen mix (21% oxygen), with slight adjustments made to the isoflurane to maintain the respiratory rate at ~ 1 Hz. Animals were kept at 37 °C with a feedback-controlled heating pad. Two photon images are average projection of three-dimensional stacks using ImageJ (NIH).

CAA burden and smooth muscle cell fragmentation in pial arteries

To quantify CAA burden and Aβ-associated fragmentation of smooth muscle cells in pial vessels [20, 31], tangential brain sections were incubated with anti-Aβ (4G8, 1:1,000, mouse; Covance) and the smooth muscle marker anti-α-actin (1:300, rabbit, Abcam) for 48 h. After washing, sections were labeled with Alexa 488-conjugated anti-rabbit IgG (1:200; Jackson ImmunoResearch) and Alexa 647-conjugated anti-rabbit IgG (1:200; Jackson ImmunoResearch). Pial arterioles ($n = 30–50$/group) positive for Aβ and α-actin, ranging in diameter from 20 to 100 µm, were randomly imaged by confocal microscope (63x). Aβ accumulation around pial-penetrating arteries was assessed by the ratio (%) between $4G8^+$ Aβ immunoreactivity and $\alpha\text{-actin}^+$ pial vessel area obtained with ImageJ in the same sections in which smooth muscle fragmentation was quantified. However, the A β specie (1–40, 1–42) was not determined. Smooth muscle cell fragmentation was quantified by counting α-actin fragments in pial-penetrating arteriole using ImageJ, expressed as the fragmentation index: 100 − [(1/number of α-actin fragments) × 100].

CAA burden in parenchymal blood vessels

CAA burden was assessed in intraparenchymal blood vessels in tangential brain sections. Brain sections were first incubated with α-actin (1:300, rabbit polyclonal; Abcam) or Glut-1 (rabbit polyclonal, 1:200, Calbiochem) antibody for 48 h, and, after washing, followed by Alexa 647-conjugated anti-rabbit IgG (1:200, Jackson ImmunoResearch). After mounting and drying on slides, brain sections were rehydrated with PBS and refixed with 4% PFA for 10 min. After washing, sections were labeled with 0.5% (wt/vol) thioflavin-S in 50% (vol/vol) ethanol for 10 min to identify CAA. Confocal images were obtained with an Alexa 488 filter for thioflavin-S and an Alexa 647 filter for α-actin or Glut-1. Images of α-actin or Glut-1 with thioflavin-S were acquired, and the number of $\alpha\text{-actin}^+$ or Glut-1^+ was quantified. The CAA burden was expressed by the number of neocortical parenchymal vessels positive for both thioflavin-S and α-actin or Glut1 [20, 31].

Brain Aβ clearance

Aβ measurement in brain and plasma

$CD36^{-/-}$ and WT mice were anesthetized with 1.5% isoflurane and placed on a stereotaxic device. A burr hole was drilled into the somatosensory cortex at coordinates: -1.58 mm anterior to bregma, 2.5 mm lateral, and 0.4 mm from the dura. Human $A\beta_{1-40}$ (100 mmol/L; rPeptide, Watkinsville, GA) was slowly injected in a volume of 1 µl using an Ultramicropump (World Precision Instruments, Sarasota, FL). One hour later blood samples were collected from the superior sagittal sinus (SSS) and heart, and the site of neocortical injection was sampled. Samples were stored at -80 °C until assay. Plasma and brain $A\beta_{1-40}$ levels were quantified using V-PLEX Aβ Peptide Panel 1 (4G8) [Stock # K15199E-2, Meso Scale Discovery (MSD), Rockville, MD, USA] according to the manufacturer instructions.

Neocortex

For determination of Aβ neocortical clearance, after surgical preparation of $CD36^{-/-}$ and WT mice, Cy5-conjugated $A\beta_{1\text{-}40}$ (100 mmol/L) was slowly injected into the neocortex at the same coordinates as above in a volume of 1 µl using an Ultramicropump (World Precision Instruments, Sarasota, FL). One hour later, brains were removed and sectioned with a vibratome (40 µm thickness) and imaged with a confocal microscope The intensity profiles of Cy5-conjugated $A\beta_{1\text{-}40}$ were quantified with ImageJ (NIH).

Striatum

For determination of Aβ clearance in the striatum [8], a guide cannula was placed in the left striatum of $CD36^{-/-}$ and WT mice at coordinates: -0.10 mm anterior to bregma, 2.2 mm lateral, and 2.8 mm from the dura. Mice were then allowed to recover for 4–6 h after surgery [8, 45]. Then, Cy5-conjugated $A\beta_{1\text{-}40}$ (1 µmol/L) was slowly injected in a volume of 0.5 µl using an injection needle. FITC labelled inulin (1 µmol/L), an inert reference molecule neither actively transported across the BBB nor retained within the brain [8, 46], was co-injected in the same mice. Thirty minutes after the co-injection, brains were sectioned in a cryostat (thickness 20 µm), and images were acquired with a confocal microscope. The intensity profiles of $A\beta_{1\text{-}40}$ and Inulin were quantified with ImageJ.

Cognitive testing

Methods for cognitive testing have been described in detail previously [33, 47, 48] and are only summarized.

Barnes maze

Mice were studied in groups of 10 with the inter-trial interval (20–30 min). All the mice examined were trained with an escape hole located in the same location across trials. No habituation trial was performed. The acquisition phase consisted of 4 consecutive training days with four trials per day. After each trial, mice remained in the escape box for 60 s before being returned to their home cages. Mice were allowed 3 min for each trial to locate the escape hole. Probe trials were performed on day 5, 24 h after the last acquisition test. After removing the escape hole, mice were placed in a start quadrant of the Barnes maze and allowed to explore for 90 s. Then, we analyzed (a) latency to enter the escape hole during the acquisition phase (escape latency) and (b) time spent in the escape quadrant in the probe trial.

Nesting test

In the evening mice were placed in individual cages with pre-weighted nestlets (3g/cage) and the next morning the remaining nestlets not assembled into a nest were weighed [49]. The nests were scored on a 5-point rating scale based on the remaining nestlet ratio and shredded conditions: 1, nestlet not noticeably torn (>90% nestlet untorn); 2, nestlet partially torn (50–90% nestlet untorn); 3, nestlet mostly shredded but not recognizable nest built (<50% nestlet untorn); 4, nest built recognizable but flat (<10% nestlet untorn); 5, nest near perfectly built like a crater (<10% nestlet untorn) with walls higher than mouse body height for more than 50% of its circumference. Shredded nestlets were expressed as %.

Statistics

Data analyses. Sample sizes were determined by power analysis using G*Power (v.3.1.9.2) based on previous works published by our lab on CBF regulation cognitive testing [25, 33]. The experiments were randomized based on the random number generator (https://www.random.org) and were performed and analyzed in a blinded fashion whenever possible. Data and image analyses were done using ImageJ 1.54c (NIH) or Prism 9 for MacOS (GraphPad Software). Data were tested for normal distribution by the D'Agostino–Person test and for outliers by the Grubbs' test (extreme studentized deviate). Two-group comparisons were analyzed using paired or unpaired two-tailed t-test, as indicated. Multiple comparisons were evaluated by one-way or two-way analysis of variance (ANOVA) and Tukey's test. Differences were considered statistically significant for probability values less than 0.05. Data are expressed as the mean ± S.E.M.

Results

Bone marrow transplantation at 12 months of age replaces leptomeningeal and perivascular BAM and not microglia

To investigate the role of BAM in CAA we used a well-established BM transplantation strategy to replace WT BAM with BAM lacking CD36 in 15-month-old Tg2576 mice with CAA. The time interval after BM transplantation determines whether the myeloid cell engraftment is limited to perivascular space and leptomeninges or involves also parenchymal microglia [24, 25, 50–53]. Some studies showed replacement of parenchymal cells few weeks after transplant in areas lacking the BBB [54]. Other studies indicated more widespread replacement in disease models [55–57]. Considering these discordant findings, we performed our own assessment of BAM replacement specifically in the Tg2576 model. To this end, we first established the time lag between BM transplantation and outcome assessment (neurovascular regulation, amyloid pathology and cognition) that restricts engraftment to BAM. After total body irradiation, we transplanted GFP^{+} BM in 3- or 12-month-old Tg2576 mice and assessed myeloid cell repopulation at

15 months of age. Age-matched littermates served as WT controls. Transplantation of GFP^+ BM resulted in accumulation of GFP^+ cells in the brain in both groups of mice. However, mice transplanted at 3 months of age and examined at 15 months exhibited, in addition to GFP^+ perivascular and leptomeningeal cells expressing the BAM marker CD206, also parenchymal GFP^+ cells with a microglial phenotype expressing high levels of Iba1 and more abundant in Tg2576 mice (Fig. 1A,C; Fig. S1A). In contrast, when 12-month-old mice were transplanted, GFP^+ cells expressing the BAM marker CD206 were observed in perivascular and leptomeningeal compartments, while $Iba1^+$ cells were GFP negative (Fig. 1B,C; Fig. S1B). No differences in the number of GFP^+CD206^+ cells were observed between Tg2576 and WT littermates transplanted at 12 months of age (Fig. 1C), confirming equal engraftment [25]. Head shielding completely prevented the repopulation of the brain by GFP^+ cells (Fig. S2) and was not used. Based on these observations in subsequent experiments mice were transplanted at 12 months of age and assessed for neurovascular physiology, amyloid pathology, and cognition at 15 months.

CD36 deletion in BAM prevents neurovascular dysfunction

We then proceeded to determine if CD36 deletion in BAM ameliorates the neurovascular dysfunction in 15 months old Tg2576 mice. First, we verified that CD36 was deleted from BAM in Tg2675 mice transplanted with $CD36^{-/-}$ BM. To this end, we studied BAM CD36 expression in WT and Tg2576 mice transplanted with $CD36^{+/+}$ (WT → WT; WT → Tg2576) or $CD36^{-/-}$ BM ($CD36^{-/-}$ → WT; $CD36^{-/-}$ → Tg2576). In WT → WT chimeras, CD36 immunoreactivity was observed in perivascular cells expressing the BAM marker CD206 (Fig. S3A,B), and was increased in WT → Tg2676 chimeras (Fig. S3A,B,E), consistent with the previously reported vascular CD36 upregulation in Tg2576 mice [30]. CD36 immunoreactivity in BAM was not observed in mice receiving $CD36^{-/-}$ BM (Fig. S3), attesting to efficient CD36 deletion in BAM. We then used laser-Doppler flowmetry to examine cerebrovascular function in 15-month-old BM chimeras anesthetized and equipped with a cranial window [30, 33, 36, 48]. First, we tested functional hyperemia, a response profoundly attenuated in Tg2576 mice [59]. As anticipated, functional hyperemia induced by mechanical stimulation of the facial whiskers was suppressed in WT → Tg2676 chimeras, compared to WT → WT (Fig. 2A), but was completely rescued in $CD36^{-/-}$ → Tg2676 chimeras. Interestingly, $CD36^{-/-}$ → WT chimeras exhibited improved functional hyperemia implicating BAM CD36 also in the attenuation of functional hyperemia observed in aging [42]. Since the ability of cerebral endothelial cells to regulate CBF is also suppressed in Tg2576 mice [60], we tested if endothelial function was also improved by $CD36^{-/-}$ BM transplantation. To this end, we studied the increase in CBF produced by bathing the exposed cerebral cortex with mechanistically distinct vasoactive agents: the endothelial nitric oxide-dependent vasodilator acetylcholine [61], the vasodilator acting through endothelial prostanoids bradykinin [62], or the receptor independent endothelium-dependent vasodilator, the Ca^{2+} ionophore A23187 [63–65]. We found that the attenuation of these endothelial responses in WT → Tg2676 was completely reversed in $CD36^{-/-}$ → Tg2676 chimeras (Fig. 2B). Finally, since CAA leads to damage and loss of SMC [31], we also tested smooth muscle vasoreactivity using the cAMP-dependent smooth muscle relaxant adenosine [66], the cGMP-dependent NO donor SNAP [67, 68], and the potent cerebrovasodilator hypercapnia ($PaCO_2$: 50-60 mmHg). CBF responses to SNAP was reduced in WT → Tg2676 and was improved in $CD36^{-/-}$ → Tg2676 chimeras (Fig. 2C). The change in the CBF response to hypercapnia did not reach statistical significance (Fig. 2D). CBF responses to adenosine were not attenuated in any group (Fig. 2D). These data demonstrate restoration of neurovascular function by BAM CD36 deletion in $CD36^{-/-}$ → Tg2676 chimeras.

CD36 deletion in BAM prevents vascular oxidative stress

The neurovascular dysfunction induced by Aβ is mediated by vascular oxidative stress [42, 69–71]. Therefore, we sought to determine if CD36 deletion in BAM suppresses ROS production in these cells. To this end, BAM were labelled by icv injection of FITC-dextran and, one day later, ROS production was assessed in BAM using DHE as a marker (Fig. 3) [25, 39]. The number of BAM did not differ between groups (Fig. 3A-C), but the increase in BAM ROS production observed in WT → Tg2676 did not occur in $CD36^{-/-}$ → Tg2676 chimeras (Fig. 3A-C). These data collectively demonstrate that deletion of CD36 in BAM suppresses ROS production in BAM in 15-month-old Tg2576 mice.

CD36 deletion in BAM ameliorates CAA without reducing amyloid plaques

Next, we examined the impact of CD36 deletion in BAM on brain Aβ and on amyloid-β accumulation in brain parenchyma and blood vessels. Brain $Aβ_{1–40}$ was reduced in $CD36^{-/-}$ → Tg2676, compared to WT → Tg2676 mice, while $Aβ_{1–42}$ was not reduced (Fig. 4A). When examining amyloid deposition, we found that parenchymal amyloid plaques were not reduced (Fig. 4B-C), but CAA was markedly attenuated both in pial and parenchymal microvessels in $CD36^{-/-}$ → Tg2676 compared to WT → Tg2676 chimeras (Fig. 5). The CAA reduction was

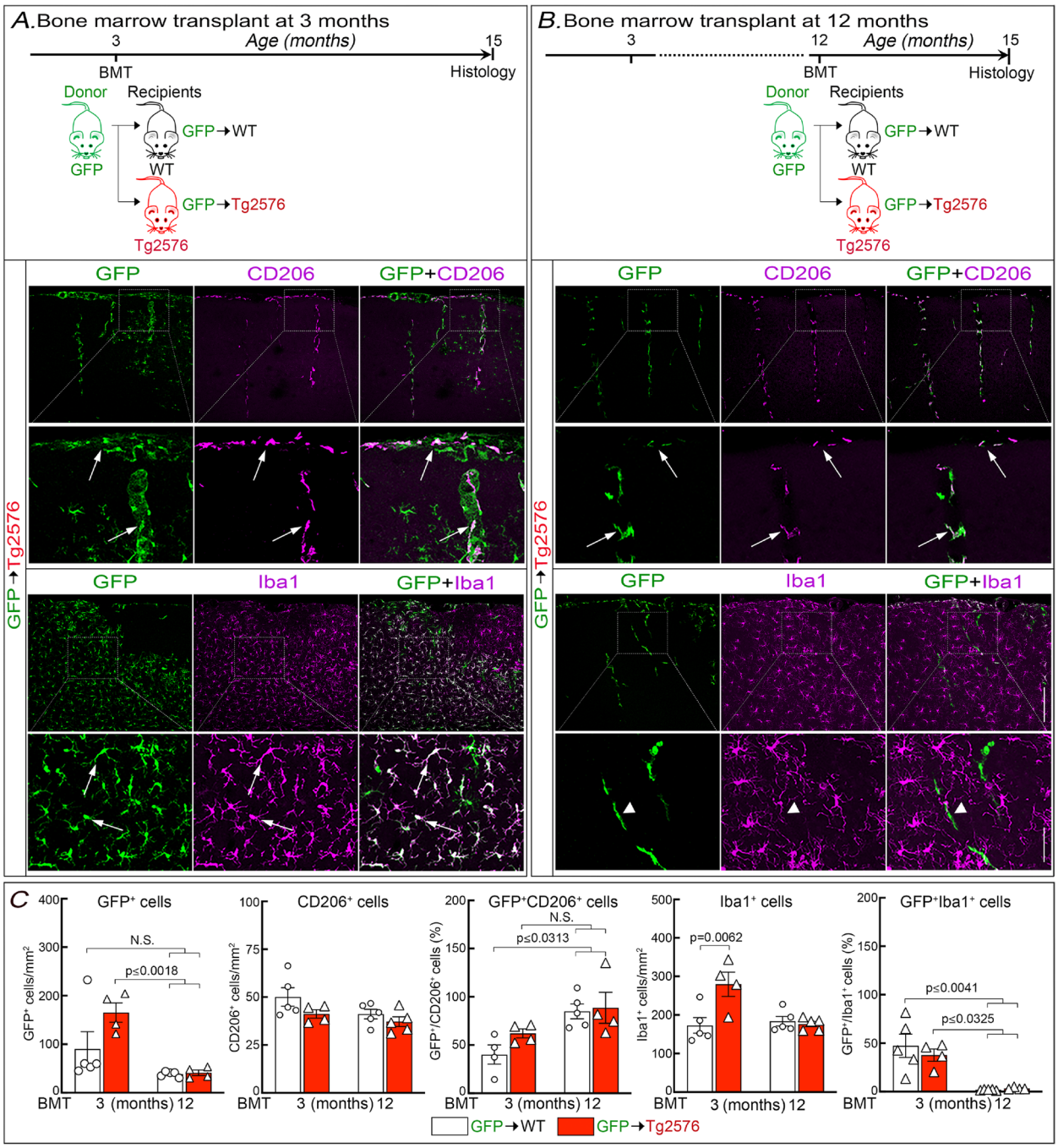

Fig. 1 Outcome of GFP$^+$ BM transplantation at 3 or 12 months of age followed by identification of GFP$^+$ cells at 15 months of age. **A** GFP$^+$ BM was transplanted into Tg2576 mice or WT littermates at 3 months and GFP$^+$ cell identity determined at 15 months of age (See Fig. S1 for WT groups). In Tg2576 mice, GFP$^+$ cells were seen surrounding cerebral blood vessels, which were also positive for the BAM marker CD206, as well in the parenchyma, which had the morphology of microglia and were strongly Iba1$^+$. **B** GFP$^+$ BM was transplanted in Tg2576 mice or WT littermates at 12 months and GFP$^+$ cell identity determined at 15 months of age. In Tg2576 mice, GFP$^+$/CD206$^+$ cells were seen surrounding cerebral blood vessels, no GFP$^+$/Iba1$^+$ were observed in the brain parenchyma. In **A**,**B**, arrows indicate co-localization and arrowheads no co-localization. **C** Number of GFP$^+$ and CD206$^+$ cells, % GFP$^+$CD206$^+$ cells, number of Iba1$^+$ cells, and % GFP$^+$/Iba1$^+$ cells at 15 months of age after BM transplant at 3 or 12 months. Of note, in agreement with a previous study [58] we did not observe an increase in microglial cels in Tg2576 mice transplanted at 12 months of age. *N* = 4–5/group; Two-way ANOVA with Tukey's test; mean ± SEM; scale bars in **A** and **B**, 200 µm and 50 µm; data presented as mean ± SEM

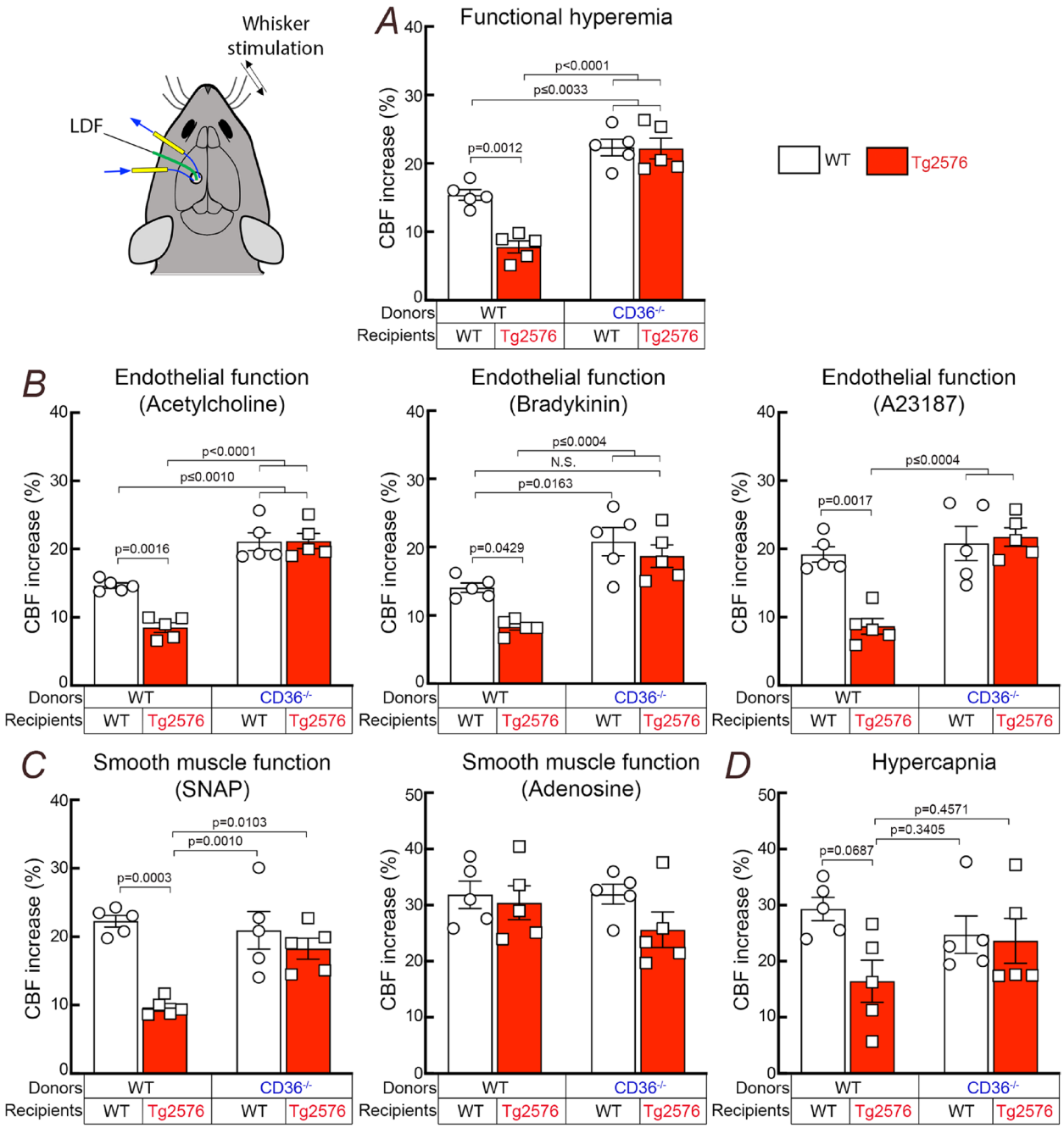

Fig. 2 Deletion of CD36 in BAM rescues neurovascular dysfunction in 15-month-old Tg2576 mice. **A** WT → Tg2576 chimeras exhibit an attenuated increase in CBF during whisker stimulation (functional hyperemia), which is completely restored in CD36$^{-/-}$ → Tg2576 chimeras. **B** CBF responses to neocortical application of the mechanistically distinct endothelium-dependent vasodilators acetylcholine, bradykinin, and the Ca^{2+} ionophore A23187 are attenuated in WT → Tg2576 chimeras and are restored in CD36$^{-/-}$ → Tg2576 chimeras. **C** The attenuation of CBF responses to neocortical application the NO donor SNAP in WT → Tg2576 is normalized in CD36$^{-/-}$ → Tg2576 chimeras. CBF responses to adenosine are not attenuated in WT → Tg2576 and remain normal in CD36$^{-/-}$ → Tg2576 chimeras **D**: CBF response to the potent vasodilator hypercapnia has a trend toward to attenuation in WT → Tg2576 which was not observed in CD36$^{-/-}$ → Tg2576 chimeras. *N* = 5/group; two-way ANOVA with Tukey's test; data presented as mean ± SEM

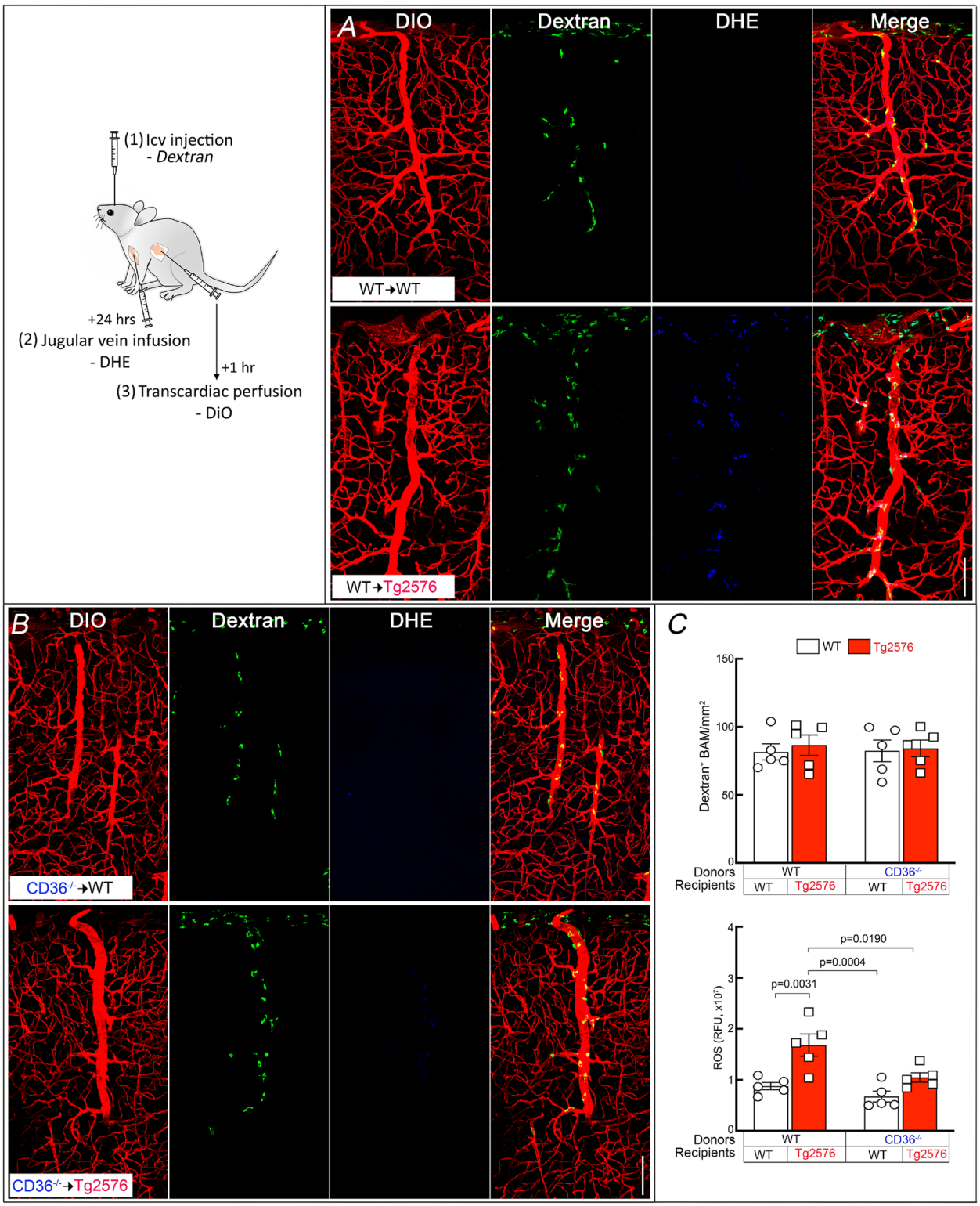

Fig. 3 CD36$^{-/-}$ BM transplant in Tg2576 mice suppresses ROS production in BAM. Mice received an icv injection of FITC-dextran to label BAM and, 24 h later, the ROS marker DHE was injected into the jugular vein. The vascular marker DiO was injected transcardiacally at the end of the experiment. **A** BAM of WT → Tg2576 mice have more DHE signal than WT → WT. **B** The DHE signal is reduced in CD36$^{-/-}$ → Tg2576 chimeras. **C** Quantification of the numbers of BAM in the BM chimeras studied showing no differences among groups (top). Quantification of the DHE signal demonstrating reduced signal in CD36$^{-/-}$ → Tg2576 chimeras (bottom). RFU: relative fluorescent units. *N* = 5/group; two-way ANOVA with Tukey's test; scale bar, 100 µm; data presented as mean ± SEM

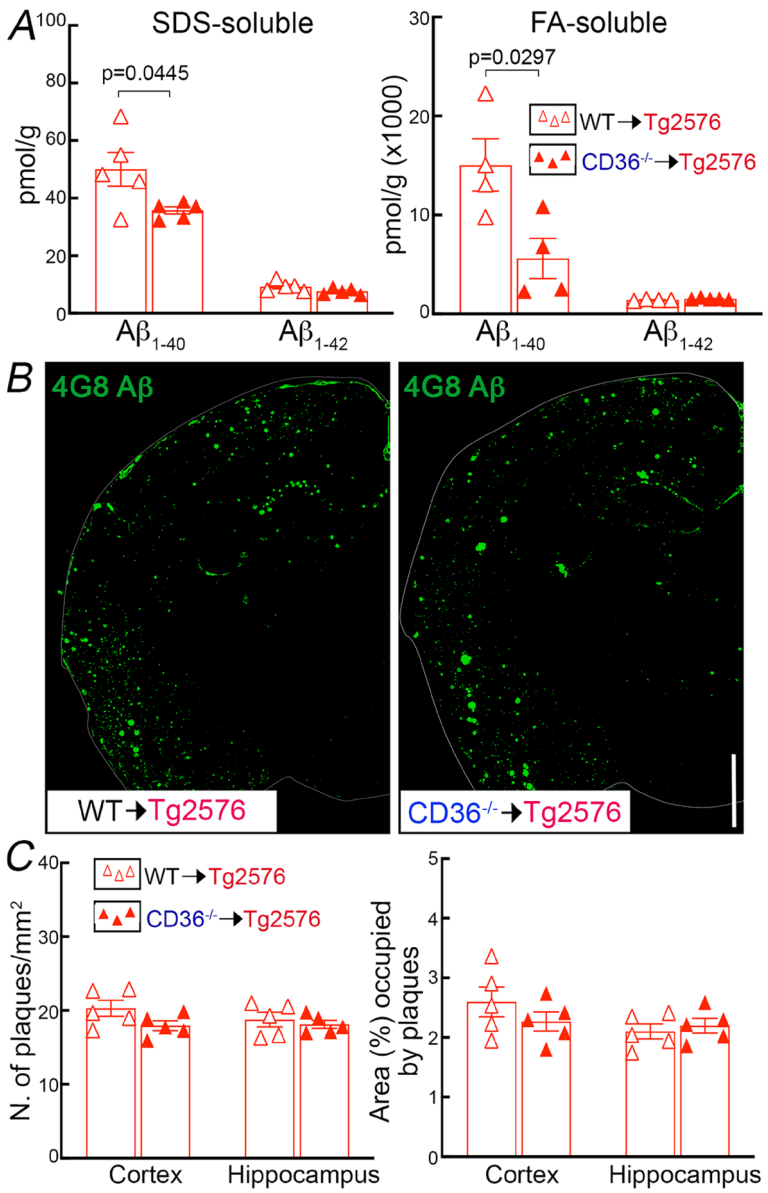

Fig. 4 Deletion of CD36 in BAM reduces $A\beta_{1\text{-}40}$, but not $A\beta_{1\text{-}42}$ or amyloid plaque load, in 15-month-old Tg2576 mice. **A** SDS-soluble and FA-soluble (SDS-insoluble) $A\beta_{1\text{-}40}$ are reduced in $CD36^{-/-}$ → Tg2576 compared with WT → Tg2576 chimeras. **B** Amyloid plaque load assessed by 4G8 immunocytochemistry. **C** Plaque number/mm^2 and percent of area occupied by plaques do not differ between WT → Tg2576 and $CD36^{-/-}$ → Tg2576. *N* = 5/group; two-way ANOVA with Tukey's test; data presented as mean ± SEM

correlated with less smooth muscle cell fragmentation and loss (Fig. 5A-C). However, the overall number of vessels assessed by Glut1 immunocytochemistry was comparable between $CD36^{-/-}$ → Tg2676 and WT → Tg2676 chimeras (Fig. 5D) suggesting that the smooth muscle cell injury was not due to global vascular degeneration. No differences in the number of $CD206^+$, $Iba1^+$, or $GFAP^+$ cells were observed between mice transplanted with WT or $CD36^{-/-}$ BM (Fig. S4). These observations, collectively, suggest CD36 deletion in BAM may promote the disposal of $A\beta_{1\text{-}40}$, the vasotropic form of the peptide, ameliorating vascular but not parenchymal Aβ deposition.

CD36 deletion in BAM rescues cognitive impairment

Next, we sought to determine if the improvement of neurovascular function and CAA in $CD36^{-/-}$ → Tg2676 chimeras was associated with improvement of cognitive function. We found that WT → Tg2676 chimeras took more time to identify the escape hole at the Barnes maze and had more difficulty identifying

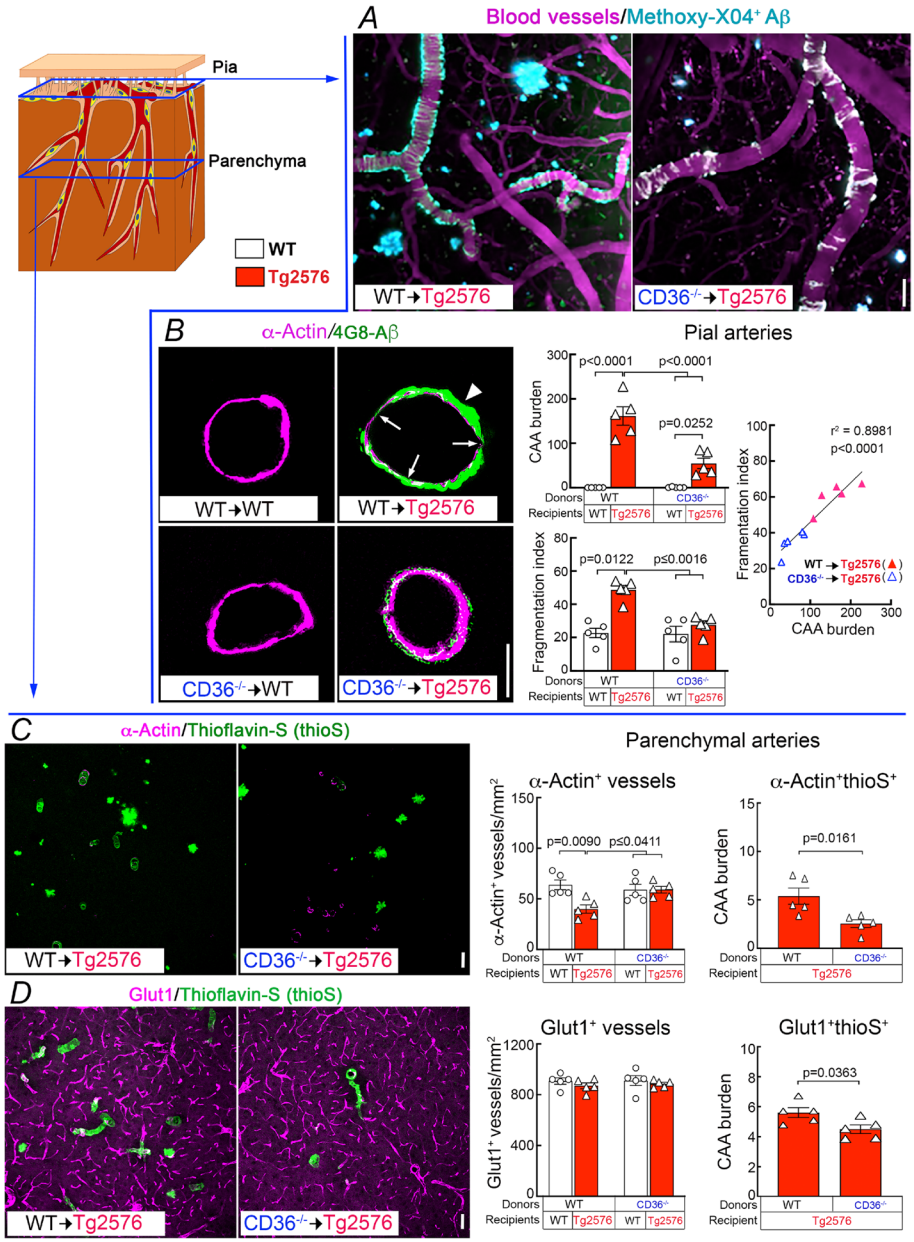

Fig. 5 CD36 deletion in BAM attenuates pial and parenchymal CAA in 15-month-old Tg2576 mice. Schematic drawing depicting the location of the pial and parenchymal vessels studied. **A-B** Pial CAA. **A** In vivo two-photon excited fluorescent images illustrating methoxy-XO4$^+$ amyloid deposits (Cyan) around somatosensory cortex blood vessels (magenta) identified by retroorbital injection of 70 kDa Texas Red dextran. Methoxy-XO4$^+$ Aβ deposits are reduced in CD36$^{-/-}$→Tg2576 compared to WT→Tg2576 mice. **B** Pial CAA burden and smooth muscle fragmentation index in tangential cortical sections double labelled with the smooth muscle cell marker α-actin and the Aβ antibody 4G8. Smooth muscle cells are fragmented (arrows) near dense amyloid deposits (CAA burden; arrowhead) in WT→Tg2576 chimeras compared with WT→WT. The barographs show quantification of CAA burden (expressed as the ratio between 4G8 and α-actin immunoreactivity) and fragmentation (see methods). The correlation plot on the right, in which the individual data points in the CAA and fragmentation barographs were correlated, shows a significant linear correlation between CAA burden and smooth muscle cell fragmentation. Reduced CAA burden in CD36$^{-/-}$→Tg2576 chimeras is associated with a comparable reduction in the fragmentation index. **C-D** Parenchymal CAA burden in tangential cortical sections double labelled with α-actin or the endothelial marker Glut1 and thioS. The barograph shows quantification of CAA burden (expressed as the number of α-actin$^+$ or Glut1$^+$ thioS$^+$ vessels/mm^2) in intraparenchymal arterioles. α-actin is reduced in WT→Tg2576 but not in CD36$^{-/-}$→Tg2576 chimeras, and the number of α-actin$^+$ thioS$^+$ vessels is reduced in CD36$^{-/-}$→Tg2576 chimeras (**C**). The number of Glut1$^+$ vessels is comparable between groups, but the number of Glut1$^+$thioS$^+$ vessels is reduced in CD36$^{-/-}$→Tg2576 chimeras (**D**). *N* = 5/group; two-way ANOVA with Tukey's test; scale bars in A-D, 50 µm. Data presented as mean ± SEM

the target quadrant once it was removed (probe test) (Fig. 6A). In contrast, CD36$^{-/-}$ → Tg2676 chimeras exhibited marked improvements in escape latency and performance at the probe test (Fig. 6A). Nest building capacity was also improved in CD36$^{-/-}$ → Tg2676 compared to WT → Tg2676 chimeras (Fig. 6B). Therefore, deletion of CD36$^{-/-}$ in BAM resulted in a marked improvement of cognitive function.

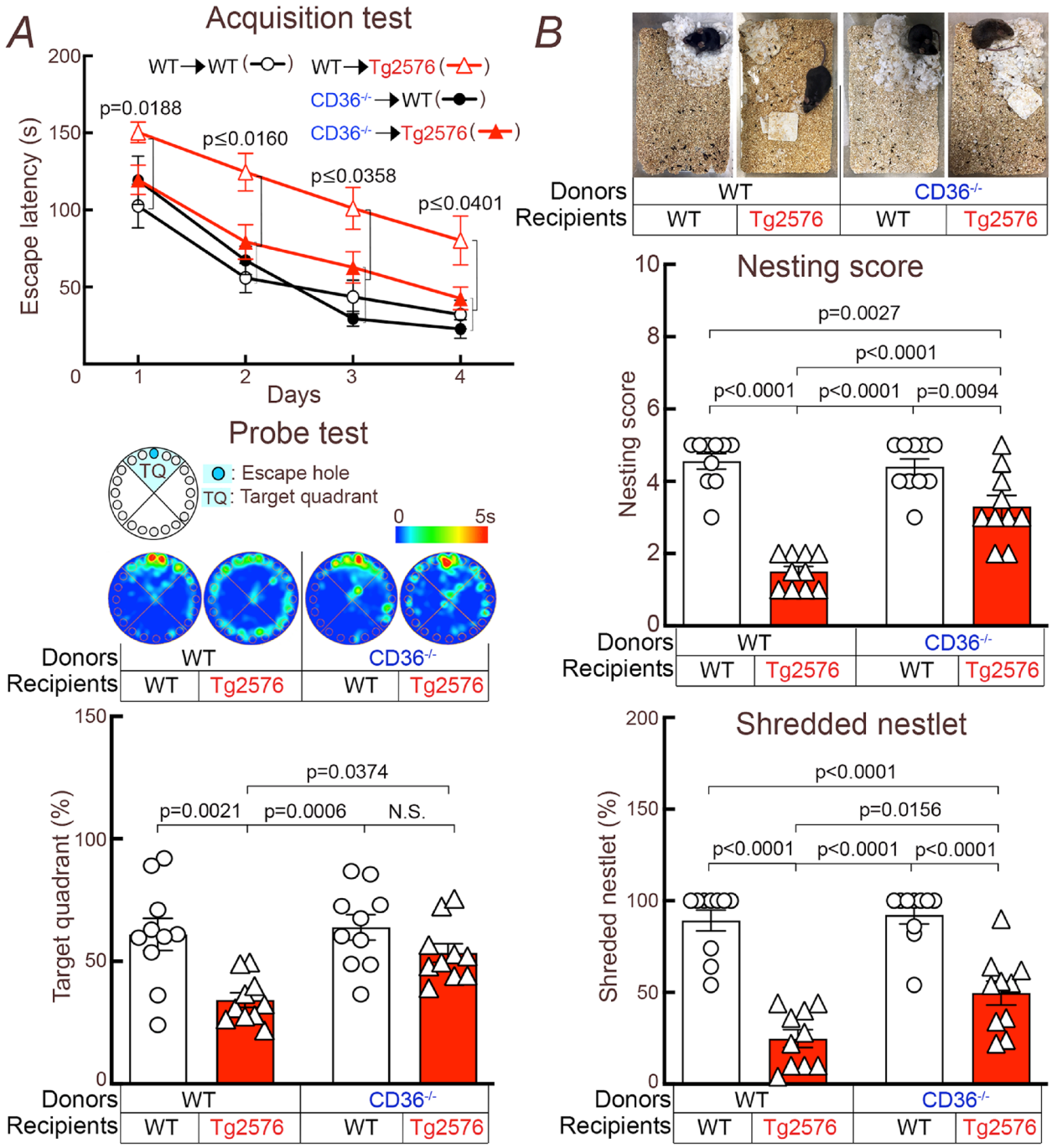

Fig. 6 CD36 deletion in BAM prevents cognitive dysfunction in 15-month-old Tg2576 mice. **A** Escape latency is increased in WT → Tg2576 and normalized in CD36$^{-/-}$ → Tg2576 chimeras. Similarly, CD36$^{-/-}$ → Tg2576 chimeras identify the target quadrant more reliably at the probe test. **B** Nest building abilities are improved in CD36$^{-/-}$ → Tg2576 chimeras, compared to WT → Tg2576 chimeras, as shown by a significantly higher nesting score and % shredded nestlets. *N* = 10/group; data were analyzed by two-way ANOVA and Tukey's test, except for the acquisition test which was analyzed by two-way ANOVA with repeated-measures and Tukey's test. Data presented as mean ± SEM

CD36 depletion promotes brain Aβ clearance

The mechanisms of amyloid accumulation in the vascular wall have not been fully elucidated, but a leading hypothesis implicates alterations in the vascular clearance of Aβ [2]. Neurovascular dysfunction impairs the elimination of Aβ from the brain by suppressing its clearance [13, 72]. Therefore, the reduction in brain $A\beta_{1-40}$ and CAA in $CD36^{-/-} \rightarrow Tg2676$ chimeras raises the possibility that CD36 deficiency promotes $A\beta_{1-40}$ clearance [73] by counteracting the well-described neurovascular dysfunction induced by $A\beta_{1-40}$. Aβ does not induce vascular ROS production and neurovascular dysfunction in $CD36^{-/-}$ mice [30, 31], and CD36 in BAM is the specific target of Aβ-induced neurovascular dysfunction and vascular ROS production [25]. Since intact neurovascular function is needed for efficient perivascular [13] and glymphatic clearance [74], it is conceivable that the reduction in vascular Aβ load in $CD36^{-/-}$ mice is related to lack of CD36 in BAM, because these cells singlehandedly mediate Aβ-induced ROS production and neurovascular dysfunction [25]. Based on these considerations, as a first approach we examined whether $CD36^{-/-}$ mice clear Aβ more efficiently. To this end, we injected Cy5-labelled $A\beta_{1-40}$ into the neocortex of WT and $CD36^{-/-}$ mice and assessed the local clearance of the tracer. We observed that Cy5- $A\beta_{1-40}$ was cleared more efficiently in $CD36^{-/-}$ than in WT mice (Fig. 7A). Thus, we found that in $CD36^{-/-}$ mice $A\beta_{1-40}$ levels were lower in the neocortex and higher in superior sagittal sinus blood, the venous effluent from the neocortex, or peripheral blood (Fig. 7B). Similarly, Cy5-$A\beta_{1-40}$ injected into the striatum was cleared more effectively in $CD36^{-/-}$ mice, while inulin, a reference marker that is neither transported across the BBB nor retained by the brain [46], was cleared equally well in WT and $CD36^{-/-}$ mice (Fig. 7C). Therefore, these initial studies suggest that $A\beta_{1-40}$ is cleared more efficiently from the brain in the absence of CD36.

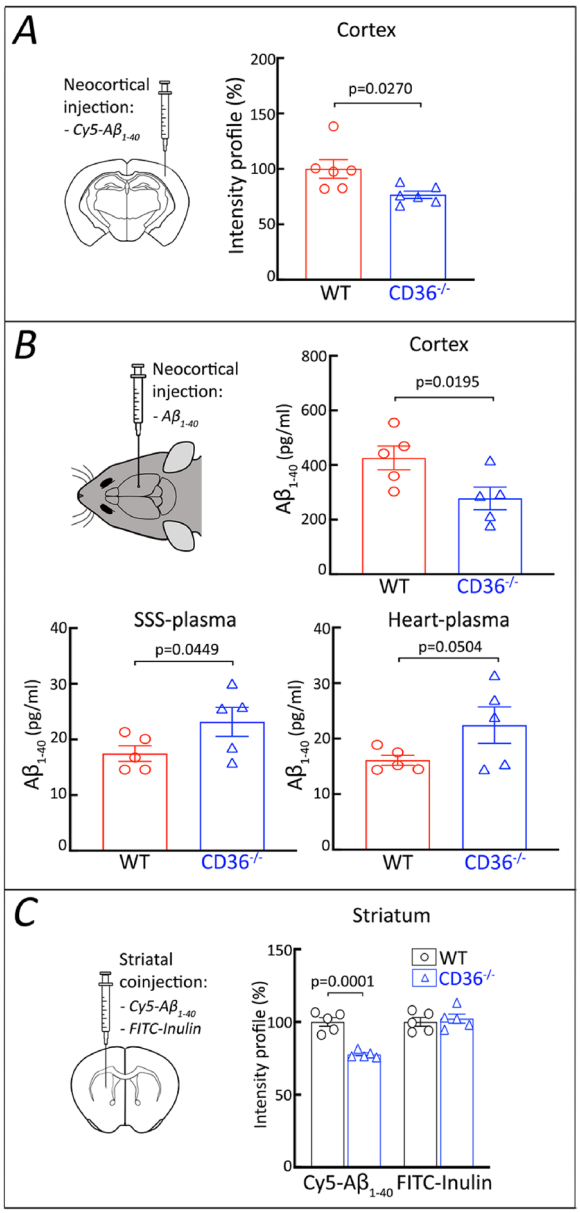

Fig. 7 $A\beta_{1-40}$ is cleared more effectively from cortex and striatum in $CD36^{-/-}$ mice than in WT mice. **A** Cy5-conjugated $A\beta_{1-40}$ was injected into the somatosensory cortex of $CD36^{-/-}$ and WT mice. One hour later, the Cy5-$A\beta_{1-40}$ fluorescence at the injection site was lower in $CD36^{-/-}$ than in WT mice. **B** Six-month-old $CD36^{-/-}$ and WT mice were injected with human $A\beta_{1-40}$ into somatosensory cortex. One hour later, $A\beta_{1-40}$ levels at the injection site were lower in CD36-/- mice, while $A\beta_{1-40}$ levels in blood sampled from the superior sagittal sinus (SSS) or the heart were higher, suggesting more efficient $A\beta_{1-40}$ tissue clearance. **C** Cy5-$A\beta_{1-40}$ and FITC-labelled inulin were co-injected into the striatum of $CD36^{-/-}$ and WT mice. Thirty min later, the Cy5-$A\beta_{1-40}$ fluorescence was lower in $CD36^{-/-}$ mice than in WT mice, while the FITC-inulin fluorescence, a reference signal, was not affected. Data were analyzed by the two-tailed unpaired T-test. Data presented as the mean ± SEM

Discussion

We investigated the role of CD36 in BAM in the neurovascular and cognitive dysfunction, and in the underlying parenchymal and vascular amyloid deposition in 15-month-old Tg2576 mice with florid amyloid pathology and cognitive impairment. After establishing and validating a BM chimera-based strategy to target BAM, we found that CD36 deletion from these cells ameliorates neurovascular dysfunction in Tg2576 mice. Loss of CD36 was associated with suppression of ROS production in BAM and reduction of brain $A\beta_{1-40}$, the Aβ species that predominates in vessels, but not $A\beta_{1-42}$, which predominates in amyloid plaques. Accordingly, neuropathological analysis demonstrated a marked reduction in arteriolar

smooth muscle cell damage and CAA, but no reduction in parenchymal amyloid plaques. The rescue of neurovascular function and the reduced oxidative stress and CAA were associated with a profound improvement of cognitive function despite the unchanged parenchymal amyloid load. These findings, collectively, unveil a previously unrecognized role of BAM in the cerebrovascular accumulation of Aβ, an effect mediated by CD36, and point to neurovascular dysfunction and CAA as critical pathogenic factors in the attendant cognitive dysfunction.

There is increasing evidence that Aβ clearance depends on cerebrovascular health [2, 6, 13]. Aβ induces major alterations in neurovascular function. In humans with sporadic CAA or with APP mutations resulting in increased brain Aβ, as in corresponding animal models, neurovascular reactivity to neural and/or endothelial stimuli is markedly suppressed [16–18, 59, 60, 75–77]. In addition, Aβ alters capillary blood flow distribution, resulting heterogeneous capillary perfusion and reduced efficiency in capillary exchange [78–80]. These deleterious neurovascular effects are in great part mediated by BAM leading to vascular oxidative stress through the CD36-Nox2 ROS-producing signaling pathway [25, 81]. In the present study, we found that CD36 deletion in BAM suppresses Aβ-induced oxidative stress, rescues key features of neurovascular function (functional hyperemia, endothelial and smooth muscle cell vasoreactivity), reduces CAA and improves cognitive function. Therefore, it is reasonable to conclude that the suppression of oxidative stress and improved neurovascular function promotes Aβ vascular clearance reducing its vascular deposition.

In support of this hypothesis exogenous Aβ injected into the brain was cleared more efficiently in CD36 null mice, as evidenced by reduced residual Aβ load in brain and increased blood Aβ in superior sagittal sinus and systemic circulation. However, total $CD36^{-/-}$ mice were used and the mice were younger than those in which CAA was assessed. Therefore, the results of these exploratory experiments need to be confirmed in mice of appropriate age with selective CD36 deletion in BAM. The recent development of $Mrc1^{CreERT2}$ driver mice for selective gene targeting in BAM [82] will facilitate this effort. The presence of anesthesia and the use of only of male mice are other limitations. These drawbacks notwithstanding, the present data provide suggestive evidence that CD36 activation by Aβ may promote vascular retention of Aβ through vascular oxidative stress and neurovascular dysfunction.

Previous studies have raised the possibility that BAM may influence brain Aβ deposition. In a mouse model of mutant APP overexpression (TgCRND8), BAM depletion by icv injection of the toxin chlodronate reduced parenchymal amyloid plaques and increased CAA [83]. In a mouse model of APP overexpression APP (J20) lacking scavenger receptor class-B type I (expressed in all myeloid cells) [84], an increase in both amyloid plaques and CAA in hippocampus was found. Furthermore, recent data suggest that BAM depletion reduces CSF clearance of Aβ and increases parenchymal amyloid load, effects linked to reduced vascular compliance and vasoreactivity [85]. While these observations would advocate for a beneficial role of BAM in preventing amyloid accumulation, our results unveil a previously unrecognized deleterious role of BAM in promoting vascular Aβ accumulation. BAM may well promote CSF clearance, but these cells once engaged by Aβ become a damaging source of vascular oxidative stress through the CD36-Nox2 pathway. Therefore, the neurovascular dysfunction and damage induced by BAM-derived ROS offsets the beneficial effects on CSF clearance.

An important translational implication of this new finding is that targeting CD36 on BAM may preserve the beneficial effects on Aβ clearance while counteracting the deleterious effect of ROS production in vascular structure and function. Cerebrovascular CD36 expression in AD brains is increased and is linked to CAA [29]. Interestingly, we also found increased vascular CD36 expression localized to BAM. Therefore, targeting BAM CD36 may be beneficial in CAA or other conditions associated with vascular amyloid accumulation such as the Amyloid-Related Imaging Abnormality (ARIA). ARIA is observed with MRI in cortical areas in up to 47% of patients receiving Aβ immunotherapy at the highest dose [86, 87]. ARIA can underlie vasogenic edema (ARIA-E), or microhemorrhages and cortical superficial siderosis (ARIA-H) [88] and is usually asymptomatic, although in some cases headache, lethargy, confusion, or behavioral changes can occur [87]. ARIA has been attributed to overload of cerebral blood vessels by Aβ peptides released from breakdown of amyloid plaque resulting in vascular dysfunction and damage [87], but recent data in a mouse model implicate vascular amyloid immunocomplexes and activation of perivascular macrophages [89]. Accumulation of perivascular macrophages ($CD163^{+}$) was also observed around Aβ-laden vessels in a patient who died after Aβ immunotherapy [90]. Since ARIA is more frequent at high doses of Aβ antibodies, which are also more effective [86, 87], counteracting ARIA may enhance the success of Aβ immunotherapy. Considering the key role of BAM CD36 in Aβ-induced vascular oxidative stress and dysfunction, and in amyloid accumulation, blocking this receptor may prove beneficial. Approaches to inhibit CD36 have been developed [91–93] and may provide the opportunity to examine their ability to

enhance vascular Aβ clearance and reduce vascular damage in a model of ARIA.

CD36 single nucleotide polymorphisms (SNP) have been linked to AD, some increasing the risk of AD [28, 94] and others delaying disease onset [94, 95]. In silico studies suggest that the protective SNP may suppress CD36-induced inflammation upon Aβ binding [95]. To our knowledge it is not known if suppressing CD36 expression reduces CAA in humans. However, as mentioned above, there is neuropathological evidence of vascular CD36 upregulation in CAA [29], which we observed in BAM. These observations strengthen the human disease relevance of the present data and point to CD36 as a putative therapeutic target for CAA and other neurovascular complications of Aβ.

A potential limitation of our study is related to the use of BM chimeras to target BAM. BM transplantation induces severe stress, acute morbidity, and leads to vascular inflammation and BBB opening [96]. However, experiments were performed 3 months after transplantation when these changes are resolved [97]. Accordingly, using this transplantation protocol WT → WT mice have normal neurovascular function, BBB permeability and cognition (present study and refs. [24–26]). Furthermore, WT → Tg2676 chimeras exhibit neurovascular, neuropathological and cognitive alterations identical to those of naïve Tg2576 mice (Present study and ref. [31]), demonstrating that the BM derived BAM repopulating the brain of Tg2576 mice have the same pathogenic effects. Strong similarities between the transcriptomic profile of BM-derived BAM repopulating the brain and that of native BAM has also been reported [52], supporting the idea that local cues determine myeloid cell identity [98]. A potential impact of radiation on CAA development or microglia is unlikely because the CAA load and microglial number are comparable to that of a previous study in which radiation was not used [31]. Even if we assume that radiation had an impact on the development of CAA, such effect would have been the same in $CD36^{+/+}$ and $CD36^{-/-}$ Tg2576 chimeras and could not explain the reduction of CAA in $CD36^{-/-}$ Tg2576 chimeras. The possibility that suppression of CD36 in circulating leukocytes plays a role in the rescue of neurovascular dysfunction in CD36 → Tg2676 chimeras is also unlikely because depletion of BAM using i.c.v. clodronate produces a similar neurovascular improvement despite the presence of CD36 in blood cells [25]. Therefore, the results of the present study cannot be attributed to confounding effects of BM transplantation.

BAM are evenly distributed along penetrating and leptomeningeal vessels, while vascular amyloid accumulates irregularly along the vessels' length with different patterns (globular, linear, ring-like) depending on the arteriolar segment [99, 100]. A common pattern of accumulation is ring-like in arteriolar smooth muscle cells [101]. Therefore, the pattern of amyloid accumulation in certain vascular segments and within the vascular wall does not match BAM localization suggesting that the ROS generated by BAM are not the proximal cause of the amyloid deposition. The leading hypothesis is that CAA results from failure of clearance of neurally-derived Aβ from the perivascular space [2, 6, 11, 102], although uptake from blood or production by mural vascular cells have also been suggested as potential mechanisms [2]. Since major pathways for perivascular clearance, i.e., retrograde perivascular and anterograde glymphatic, depend on efficient neurovascular function [13, 74], the neurovascular dysfunction induced by BAM-generated ROS is likely to be the cause of impaired Aβ clearance and subsequent accumulation. Our finding that Aβ clearance is enhanced in the absence of CD36, with the well-acknowledged limitations mentioned above, supports the contention that the neurovascular dysfunction induced by CD36-Nox2-dependent ROS production is responsible for reduced Aβ clearance. Why Aβ accumulates only at selected sites in different morphological patterns remains to be established and depend on a variety of factors. These may include (a) the hydrodynamics of CSF outflow from the perivascular space, (b) Aβ species and concentration, which may explain why the heaviest accumulation is observed in intracortical vessels where neurally-derived Aβ is thought to be more concentrated [100], (c) the geometry of the perivascular space, which are more tortuous and convoluted in CAA [101], (d) the ApoE status [101], and (e) Aβ seeding and deposition into smooth muscle and other mural cells [103].

Conclusions

We have investigated the role of CD36 in BAM in a mouse model of CAA. First, we established a BM transplantation-based strategy to selectively delete CD36 from BAM in 15-month-old Tg2576 mice with extensive CAA and cognitive impairment. Using this approach, we found that CD36 deletion in BAM suppresses free radical production in these cells and rescues the neurovascular dysfunction induced by Aβ. CD36 deletion in BAM also reduced brain $Aβ_{1-40}$, prevented microvascular smooth muscle cell damage, and ameliorated CAA without affecting parenchyma plaques. Lack of CD36 enhanced the vascular clearance of exogenous Aβ. These beneficial vascular effects resulted in a near complete rescue of cognitive function in 15-month-old Tg2576 mice. Collectively, these data implicate CD36 in BAM in the accumulation of Aβ in cerebral blood vessels and raise the possibility that targeting BAM CD36 is a new therapeutic approach for CAA and other conditions associated with vascular Aβ deposition and damage.

Supplementary Information

The online version contains supplementary material available at https://doi.org/10.1186/s13024-023-00660-1.

Additional file 1.

Acknowledgements
Support from the Feil Family Foundation is gratefully acknowledged.

Authors' contributions
KU, LP, and CI designed the study and performed the primary interpretation of the data; KU, YH, SJA, JS, NC, AA, and LP conducted the experiments; KU, YH, SJA, LP and CI performed the data analysis; SJA conducted the two-photon microscopy; WL provided resources for Aβ measurement; PZ, JA, LP, and CI supervised the research; LP and CI provided funding and wrote the first draft of the manuscript. All authors contributed and critically reviewed the final version of the manuscript. All authors read and approved the final manuscript.

Funding
Supported by NIH grants R01-NS37853 (CI), R01-NS097805 (LP), Japan Heart Foundation/Bayer Research Grant Abroad (YH), The Uehara Memorial Foundation Research Fellowship (YH), and Japan Society for the Promotion of Science Overseas Research Fellowships (YH), the Leon Levy Foundation (SJA), and the BrightFocus foundation (AA).

Availability of data and materials
All data generated or analyzed during this study are included in this published article and its additional files.

Declarations

Ethics approval and consent to participate
All procedures were approved by the Institutional Animal Care and Use Committee of Weill Cornell Medicine and performed according to the ARRIVE guidelines.

Consent for publication
N/A.

Competing interests
None.

Author details
[1]Feil Family Brain and Mind Research Institute, Weill Cornell Medicine, New York, NY 10021, USA.

Received: 27 March 2023 Accepted: 20 September 2023
Published online: 03 October 2023

References

1. Attems J. Sporadic cerebral amyloid angiopathy: pathology, clinical implications, and possible pathomechanisms. Acta Neuropathol. 2005;110:345–59.
2. Greenberg SM, Bacskai BJ, Hernandez-Guillamon M, Pruzin J, Sperling R, van Veluw SJ. Cerebral amyloid angiopathy and Alzheimer disease - one peptide, two pathways. Nat Rev Neurol. 2020;16:30–42.
3. Gravina SA, Ho L, Eckman CB, Long KE, Otvos L Jr, Younkin LH, Younkin SG. Amyloid beta protein (A beta) in Alzheimer's disease brain. Biochemical and immunocytochemical analysis with antibodies specific for forms ending at A beta 40 or A beta 42(43). J Biol Chem. 1995;270:7013–6.
4. Kakuda N, Miyasaka T, Iwasaki N, Nirasawa T, Wada-Kakuda S, Takahashi-Fujigasaki J, Murayama S, Ihara Y, Ikegawa M. Distinct deposition of amyloid-beta species in brains with Alzheimer's disease pathology visualized with MALDI imaging mass spectrometry. Acta Neuropathol Commun. 2017;5:73.
5. Miller DL, Papayannopoulos IA, Styles J, Bobin SA, Lin YY, Biemann K, Iqbal K. Peptide compositions of the cerebrovascular and senile plaque core amyloid deposits of Alzheimer's disease. Arch Biochem Biophys. 1993;301:41–52.
6. Tarasoff-Conway JM, Carare RO, Osorio RS, Glodzik L, Butler T, Fieremans E, Axel L, Rusinek H, Nicholson C, Zlokovic BV, et al. Clearance systems in the brain-implications for Alzheimer disease. Nat Rev Neurol. 2015;11:457–70.
7. Bell RD, Sagare AP, Friedman AE, Bedi GS, Holtzman DM, Deane R, Zlokovic BV. Transport pathways for clearance of human Alzheimer's amyloid beta-peptide and apolipoproteins E and J in the mouse central nervous system. J Cereb Blood Flow Metab. 2007;27:909–18.
8. Cirrito JR, Deane R, Fagan AM, Spinner ML, Parsadanian M, Finn MB, Jiang H, Prior JL, Sagare A, Bales KR, et al. P-glycoprotein deficiency at the blood-brain barrier increases amyloid-beta deposition in an Alzheimer disease mouse model. J Clin Invest. 2005;115:3285–90.
9. Deane R, Wu Z, Sagare A, Davis J, Du Yan S, Hamm K, Xu F, Parisi M, LaRue B, Hu HW, et al. LRP/amyloid beta-peptide interaction mediates differential brain efflux of Abeta isoforms. Neuron. 2004;43:333–44.
10. Albargothy NJ, Johnston DA, MacGregor-Sharp M, Weller RO, Verma A, Hawkes CA, Carare RO. Convective influx/glymphatic system: tracers injected into the CSF enter and leave the brain along separate periarterial basement membrane pathways. Acta Neuropathol. 2018;136:139–52.
11. Chen X, Liu X, Koundal S, Elkin R, Zhu X, Monte B, Xu F, Dai F, Pedram M, Lee H, et al. Cerebral amyloid angiopathy is associated with glymphatic transport reduction and time-delayed solute drainage along the neck arteries. Nat Aging. 2022;2:214–23.
12. Kress BT, Iliff JJ, Xia M, Wang M, Wei HS, Zeppenfeld D, Xie L, Kang H, Xu Q, Liew JA, et al. Impairment of paravascular clearance pathways in the aging brain. Ann Neurol. 2014;76:845–61.
13. van Veluw SJ, Hou SS, Calvo-Rodriguez M, Arbel-Ornath M, Snyder AC, Frosch MP, Greenberg SM, Bacskai BJ. Vasomotion as a Driving Force for Paravascular Clearance in the Awake Mouse Brain. Neuron. 2020;105:549–61.
14. Da Mesquita S, Louveau A, Vaccari A, Smirnov I, Cornelison RC, Kingsmore KM, Contarino C, Onengut-Gumuscu S, Farber E, Raper D, et al. Functional aspects of meningeal lymphatics in ageing and Alzheimer's disease. Nature. 2018;560:185–91.
15. Schaeffer S, Iadecola C. Revisiting the neurovascular unit. Nat Neurosci. 2021;24:1198–209.
16. Dumas A, Dierksen GA, Gurol ME, Halpin A, Martinez-Ramirez S, Schwab K, Rosand J, Viswanathan A, Salat DH, Polimeni JR, Greenberg SM. Functional magnetic resonance imaging detection of vascular reactivity in cerebral amyloid angiopathy. Ann Neurol. 2012;72:76–81.
17. Peca S, McCreary CR, Donaldson E, Kumarpillai G, Shobha N, Sanchez K, Charlton A, Steinback CD, Beaudin AE, Fluck D, et al. Neurovascular decoupling is associated with severity of cerebral amyloid angiopathy. Neurology. 2013;81:1659–65.
18. Smith EE, Vijayappa M, Lima F, Delgado P, Wendell L, Rosand J, Greenberg SM. Impaired visual evoked flow velocity response in cerebral amyloid angiopathy. Neurology. 2008;71:1424–30.
19. Han BH, Zhou ML, Johnson AW, Singh I, Liao F, Vellimana AK, Nelson JW, Milner E, Cirrito JR, Basak J, et al. Contribution of reactive oxygen species to cerebral amyloid angiopathy, vasomotor dysfunction, and microhemorrhage in aged Tg2576 mice. Proc Natl Acad Sci U S A. 2015;112:E881-890.
20. Park L, Koizumi K, El Jamal S, Zhou P, Previti ML, Van Nostrand WE, Carlson G, Iadecola C. Age-dependent neurovascular dysfunction and damage in a mouse model of cerebral amyloid angiopathy. Stroke. 2014;45:1815–21.
21. Vargas-Soria M, Ramos-Rodriguez JJ, Del Marco A, Hierro-Bujalance C, Carranza-Naval MJ, Calvo-Rodriguez M, van Veluw SJ, Stitt AW, Simo R, Backskai BJ, et al. Accelerated amyloid angiopathy and related vascular alterations in a mixed murine model of Alzheimer s disease and type two diabetes. Fluids Barriers CNS. 2022;19:88.
22. Ojo JO, Reed JM, Crynen G, Vallabhaneni P, Evans J, Shackleton B, Eisenbaum M, Ringland C, Edsell A, Mullan M, et al. Molecular Pathobiology of the Cerebrovasculature in Aging and in Alzheimers Disease Cases

With Cerebral Amyloid Angiopathy. Front Aging Neurosci. 2021;13:658605.
23. Masuda T, Amann L, Monaco G, Sankowski R, Staszewski O, Krueger M, Del Gaudio F, He L, Paterson N, Nent E, et al. Specification of CNS macrophage subsets occurs postnatally in defined niches. Nature. 2022;604:740–8.
24. Faraco G, Sugiyama Y, Lane D, Garcia-Bonilla L, Chang H, Santisteban MM, Racchumi G, Murphy M, Van Rooijen N, Anrather J, Iadecola C. Perivascular macrophages mediate the neurovascular and cognitive dysfunction associated with hypertension. J Clin Invest. 2016;126:4674–89.
25. Park L, Uekawa K, Garcia-Bonilla L, Koizumi K, Murphy M, Pitstick R, Younkin LH, Younkin SG, Zhou P, Carlson GA, et al. Brain Perivascular Macrophages Initiate the Neurovascular Dysfunction of Alzheimer Abeta Peptides. Circ Res. 2017;121:258–69.
26. Santisteban MM, Ahn SJ, Lane D, Faraco G, Garcia-Bonilla L, Racchumi G, Poon C, Schaeffer S, Segarra SG, Korbelin J, et al. Endothelium-Macrophage Crosstalk Mediates Blood-Brain Barrier Dysfunction in Hypertension. Hypertension. 2020;76:795–807.
27. Dobri AM, Dudau M, Enciu AM, Hinescu ME. CD36 in Alzheimer's Disease: An Overview of Molecular Mechanisms and Therapeutic Targeting. Neuroscience. 2021;453:301–11.
28. Sery O, Janoutova J, Ewerlingova L, Halova A, Lochman J, Janout V, Khan NA, Balcar VJ. CD36 gene polymorphism is associated with Alzheimer's disease. Biochimie. 2017;135:46–53.
29. Wilhelmus MM, Otte-Holler I, van Triel JJ, Veerhuis R, Maat-Schieman ML, Bu G, de Waal RM, Verbeek MM. Lipoprotein receptor-related protein-1 mediates amyloid-beta-mediated cell death of cerebrovascular cells. Am J Pathol. 2007;171:1989–99.
30. Park L, Wang G, Zhou P, Zhou J, Pitstick R, Previti ML, Younkin L, Younkin SG, Van Nostrand WE, Cho S, et al. Scavenger receptor CD36 is essential for the cerebrovascular oxidative stress and neurovascular dysfunction induced by amyloid-beta. Proc Natl Acad Sci U S A. 2011;108:5063–8.
31. Park L, Zhou J, Zhou P, Pistick R, El Jamal S, Younkin L, Pierce J, Arreguin A, Anrather J, Younkin SG, et al. Innate immunity receptor CD36 promotes cerebral amyloid angiopathy. Proc Natl Acad Sci U S A. 2013;110:3089–94.
32. Hsiao K, Chapman P, Nilsen S, Eckman C, Harigaya Y, Younkin S, Yang F, Cole G. Correlative memory deficits, Abeta elevation, and amyloid plaques in transgenic mice. Science. 1996;274:99–102.
33. Park L, Hochrainer K, Hattori Y, Ahn SJ, Anfray A, Wang G, Uekawa K, Seo J, Palfini V, Blanco I, et al. Tau induces PSD95-neuronal NOS uncoupling and neurovascular dysfunction independent of neurodegeneration. Nat Neurosci. 2020;23:1079–89.
34. Park L, Zhou J, Koizumi K, Wang G, Anfray A, Ahn SJ, Seo J, Zhou P, Zhao L, Paul S, et al. tPA Deficiency Underlies Neurovascular Coupling Dysfunction by Amyloid-beta. J Neurosci. 2020;40:8160–73.
35. Garcia-Bonilla L, Racchumi G, Murphy M, Anrather J, Iadecola C. Endothelial CD36 Contributes to Postischemic Brain Injury by Promoting Neutrophil Activation via CSF3. J Neurosci. 2015;35:14783–93.
36. Iadecola C. Nitric oxide participates in the cerebrovasodilation elicited from cerebellar fastigial nucleus. Am J Physiol. 1992;263:R1156-1161.
37. Park L, Wang G, Moore J, Girouard H, Zhou P, Anrather J, Iadecola C. The key role of transient receptor potential melastatin-2 channels in amyloid-beta-induced neurovascular dysfunction. Nat Commun. 2014;5:5318.
38. Carare RO, Bernardes-Silva M, Newman TA, Page AM, Nicoll JA, Perry VH, Weller RO. Solutes, but not cells, drain from the brain parenchyma along basement membranes of capillaries and arteries: significance for cerebral amyloid angiopathy and neuroimmunology. Neuropathol Appl Neurobiol. 2008;34:131–44.
39. Li Y, Song Y, Zhao L, Gaidosh G, Laties AM, Wen R. Direct labeling and visualization of blood vessels with lipophilic carbocyanine dye DiI. Nat Protoc. 2008;3:1703–8.
40. Goldmann T, Wieghofer P, Jordao MJ, Prutek F, Hagemeyer N, Frenzel K, Amann L, Staszewski O, Kierdorf K, Krueger M, et al. Origin, fate and dynamics of macrophages at central nervous system interfaces. Nat Immunol. 2016;17:797–805.
41. Polfliet MM, Goede PH, van Kesteren-Hendrikx EM, van Rooijen N, Dijkstra CD, van den Berg TK. A method for the selective depletion of perivascular and meningeal macrophages in the central nervous system. J Neuroimmunol. 2001;116:188–95.
42. Park L, Anrather J, Girouard H, Zhou P, Iadecola C. Nox2-derived reactive oxygen species mediate neurovascular dysregulation in the aging mouse brain. J Cereb Blood Flow Metab. 2007;27:1908–18.
43. Park L, Zhou P, Pitstick R, Capone C, Anrather J, Norris EH, Younkin L, Younkin S, Carlson G, McEwen BS, Iadecola C. Nox2-derived radicals contribute to neurovascular and behavioral dysfunction in mice overexpressing the amyloid precursor protein. Proc Natl Acad Sci U S A. 2008;105:1347–52.
44. Klunk WE, Bacskai BJ, Mathis CA, Kajdasz ST, McLellan ME, Frosch MP, Debnath ML, Holt DP, Wang Y, Hyman BT. Imaging Abeta plaques in living transgenic mice with multiphoton microscopy and methoxy-X04, a systemically administered Congo red derivative. J Neuropathol Exp Neurol. 2002;61:797–805.
45. Cirrito JR, May PC, O'Dell MA, Taylor JW, Parsadanian M, Cramer JW, Audia JE, Nissen JS, Bales KR, Paul SM, et al. In vivo assessment of brain interstitial fluid with microdialysis reveals plaque-associated changes in amyloid-beta metabolism and half-life. J Neurosci. 2003;23:8844–53.
46. Hladky SB, Barrand MA. Elimination of substances from the brain parenchyma: efflux via perivascular pathways and via the blood-brain barrier. Fluids Barriers CNS. 2018;15:30.
47. Faraco G, Brea D, Garcia-Bonilla L, Wang G, Racchumi G, Chang H, Buendia I, Santisteban MM, Segarra SG, Koizumi K, et al. Dietary salt promotes neurovascular and cognitive dysfunction through a gut-initiated TH17 response. Nat Neurosci. 2018;21:240–9.
48. Koizumi K, Hattori Y, Ahn SJ, Buendia I, Ciacciarelli A, Uekawa K, Wang G, Hiller A, Zhao L, Voss HU, et al. Apoepsilon4 disrupts neurovascular regulation and undermines white matter integrity and cognitive function. Nat Commun. 2018;9:3816.
49. Deacon RM. Assessing nest building in mice. Nat Protoc. 2006;1:1117–9.
50. Mildner A, Schlevogt B, Kierdorf K, Bottcher C, Erny D, Kummer MP, Quinn M, Bruck W, Bechmann I, Heneka MT, et al. Distinct and non-redundant roles of microglia and myeloid subsets in mouse models of Alzheimer's disease. J Neurosci. 2011;31:11159–71.
51. Mildner A, Schmidt H, Nitsche M, Merkler D, Hanisch UK, Mack M, Heikenwalder M, Bruck W, Priller J, Prinz M. Microglia in the adult brain arise from Ly-6ChiCCR2+ monocytes only under defined host conditions. Nat Neurosci. 2007;10:1544–53.
52. Shemer A, Grozovski J, Tay TL, Tao J, Volaski A, Suss P, Ardura-Fabregat A, Gross-Vered M, Kim JS, David E, et al. Engrafted parenchymal brain macrophages differ from microglia in transcriptome, chromatin landscape and response to challenge. Nat Commun. 2018;9:5206.
53. Vallieres L, Sawchenko PE. Bone marrow-derived cells that populate the adult mouse brain preserve their hematopoietic identity. J Neurosci. 2003;23:5197–207.
54. Urabe H, Kojima H, Chan L, Terashima T, Ogawa N, Katagi M, Fujino K, Kumagai A, Kawai H, Asakawa A, et al. Haematopoietic cells produce BDNF and regulate appetite upon migration to the hypothalamus. Nat Commun. 2013;4:1526.
55. Hess DC, Abe T, Hill WD, Studdard AM, Carothers J, Masuya M, Fleming PA, Drake CJ, Ogawa M. Hematopoietic origin of microglial and perivascular cells in brain. Exp Neurol. 2004;186:134–44.
56. Malm TM, Koistinaho M, Parepalo M, Vatanen T, Ooka A, Karlsson S, Koistinaho J. Bone-marrow-derived cells contribute to the recruitment of microglial cells in response to beta-amyloid deposition in APP/PS1 double transgenic Alzheimer mice. Neurobiol Dis. 2005;18:134–42.
57. Simard AR, Soulet D, Gowing G, Julien JP, Rivest S. Bone marrow-derived microglia play a critical role in restricting senile plaque formation in Alzheimer's disease. Neuron. 2006;49:489–502.
58. Nichol KE, Poon WW, Parachikova AI, Cribbs DH, Glabe CG, Cotman CW. Exercise alters the immune profile in Tg2576 Alzheimer mice toward a response coincident with improved cognitive performance and decreased amyloid. J Neuroinflammation. 2008;5:13.
59. Niwa K, Younkin L, Ebeling C, Turner SK, Westaway D, Younkin S, Ashe KH, Carlson GA, Iadecola C. Abeta 1–40-related reduction in functional hyperemia in mouse neocortex during somatosensory activation. Proc Natl Acad Sci U S A. 2000;97:9735–40.
60. Iadecola C, Zhang F, Niwa K, Eckman C, Turner SK, Fischer E, Younkin S, Borchelt DR, Hsiao KK, Carlson GA. SOD1 rescues cerebral endothelial

dysfunction in mice overexpressing amyloid precursor protein. Nat Neurosci. 1999;2:157–61.
61. Toda N, Ayajiki K, Okamura T. Cerebral blood flow regulation by nitric oxide: recent advances. Pharmacol Rev. 2009;61:62–97.
62. Niwa K, Haensel C, Ross ME, Iadecola C. Cyclooxygenase-1 participates in selected vasodilator responses of the cerebral circulation. Circ Res. 2001;88:600–8.
63. Rosenblum WI. Hydroxyl radical mediates the endothelium-dependent relaxation produced by bradykinin in mouse cerebral arterioles. Circ Res. 1987;61:601–3.
64. Rosenblum WI, McDonald M, Wormley B. Calcium ionophore and acetylcholine dilate arterioles on the mouse brain by different mechanisms. Stroke. 1989;20:1391–5.
65. Sobey CG, Heistad DD, Faraci FM. Mechanisms of bradykinin-induced cerebral vasodilatation in rats. Evidence that reactive oxygen species activate K+ channels. Stroke. 1997;28:2290–4.
66. Faraci FM, Heistad DD. Regulation of the cerebral circulation: role of endothelium and potassium channels. Physiol Rev. 1998;78:53–97.
67. Wang Q, Pelligrino DA, Koenig HM, Albrecht RF. The role of endothelium and nitric oxide in rat pial arteriolar dilatory responses to CO2 in vivo. J Cereb Blood Flow Metab. 1994;14:944–51.
68. Yang G, Zhang Y, Ross ME, Iadecola C. Attenuation of activity-induced increases in cerebellar blood flow in mice lacking neuronal nitric oxide synthase. Am J Physiol Heart Circ Physiol. 2003;285:H298-304.
69. Park L, Anrather J, Forster C, Kazama K, Carlson GA, Iadecola C. Abeta-induced vascular oxidative stress and attenuation of functional hyperemia in mouse somatosensory cortex. J Cereb Blood Flow Metab. 2004;24:334–42.
70. Park L, Anrather J, Zhou P, Frys K, Pitstick R, Younkin S, Carlson GA, Iadecola C. NADPH-oxidase-derived reactive oxygen species mediate the cerebrovascular dysfunction induced by the amyloid beta peptide. J Neurosci. 2005;25:1769–77.
71. Tong XK, Nicolakakis N, Kocharyan A, Hamel E. Vascular remodeling versus amyloid beta-induced oxidative stress in the cerebrovascular dysfunctions associated with Alzheimer's disease. J Neurosci. 2005;25:11165–74.
72. Sagare AP, Bell RD, Zlokovic BV. Neurovascular dysfunction and faulty amyloid beta-peptide clearance in Alzheimer disease. Cold Spring Harb Perspect Med. 2012;2:a011452.
73. Shibata M, Yamada S, Kumar SR, Calero M, Bading J, Frangione B, Holtzman DM, Miller CA, Strickland DK, Ghiso J, Zlokovic BV. Clearance of Alzheimer's amyloid-ss(1–40) peptide from brain by LDL receptor-related protein-1 at the blood-brain barrier. J Clin Investig. 2000;106:1489–99.
74. Holstein-Ronsbo S, Gan Y, Giannetto MJ, Rasmussen MK, Sigurdsson B, Beinlich FRM, Rose L, Untiet V, Hablitz LM, Kelley DH, Nedergaard M. Glymphatic influx and clearance are accelerated by neurovascular coupling. Nat Neurosci. 2023;26:1042–53.
75. Janik R, Thomason LA, Chaudhary S, Dorr A, Scouten A, Schwindt G, Masellis M, Stanisz GJ, Black SE, Stefanovic B. Attenuation of functional hyperemia to visual stimulation in mild Alzheimer's disease and its sensitivity to cholinesterase inhibition. Biochim Biophys Acta. 2016;1862:957–65.
76. McDade E, Kim A, James J, Sheu LK, Kuan DC, Minhas D, Gianaros PJ, Ikonomovic S, Lopez O, Snitz B, et al. Cerebral perfusion alterations and cerebral amyloid in autosomal dominant Alzheimer disease. Neurology. 2014;83:710–7.
77. Smith CD, Andersen AH, Kryscio RJ, Schmitt FA, Kindy MS, Blonder LX, Avison MJ. Altered brain activation in cognitively intact individuals at high risk for Alzheimer's disease. Neurol. 1999;53:1391–6.
78. Cruz Hernandez JC, Bracko O, Kersbergen CJ, Muse V, Haft-Javaherian M, Berg M, Park L, Vinarcsik LK, Ivasyk I, Rivera DA, et al. Neutrophil adhesion in brain capillaries reduces cortical blood flow and impairs memory function in Alzheimer's disease mouse models. Nat Neurosci. 2019;22:413–20.
79. Nortley R, Korte N, Izquierdo P, Hirunpattarasilp C, Mishra A, Jaunmuktane Z, Kyrargyri V, Pfeiffer T, Khennouf L, Madry C, et al. Amyloid beta oligomers constrict human capillaries in Alzheimer's disease via signaling to pericytes. Science. 2019;365:eaav9518.
80. Ostergaard L. Blood flow, capillary transit times, and tissue oxygenation: the centennial of capillary recruitment. J Appl Physiol. 1985;2020(129):1413–21.
81. Ruiz-Uribe NE, Bracko O, Swallow M, Omurzakov A, Dash S, Uchida H, Xiang D, Haft-Javaherian M, Falkenhain K, Lamont ME, et al: Vascular oxidative stress causes neutrophil arrest in brain capillaries, leading to decreased cerebral blood flow and contributing to memory impairment in a mouse model of Alzheimer's disease. bioRxiv 2023.
82. Anfray A, Schaeffer S, Hattori Y, Santisteban M, Casey N, Wang G, Strickland M, Zhou P, Holtzman DM, Anrather J, et al: Cell autonomous role of border associated macrophages in ApoE4 neurovascular dysfunction and susceptibility to white matter injury Res Sq 2023:rs.3.rs-3222611.
83. Hawkes CA, McLaurin J. Selective targeting of perivascular macrophages for clearance of beta-amyloid in cerebral amyloid angiopathy. Proc Natl Acad Sci U S A. 2009;106:1261–6.
84. Thanopoulou K, Fragkouli A, Stylianopoulou F, Georgopoulos S. Scavenger receptor class B type I (SR-BI) regulates perivascular macrophages and modifies amyloid pathology in an Alzheimer mouse model. Proc Natl Acad Sci U S A. 2010;107:20816–21.
85. Drieu A, Du S, Storck SE, Rustenhoven J, Papadopoulos Z, Dykstra T, Zhong F, Kim K, Blackburn S, Mamuladze T, et al. Parenchymal border macrophages regulate the flow dynamics of the cerebrospinal fluid. Nature. 2022;611:585–93.
86. Sevigny J, Chiao P, Bussiere T, Weinreb PH, Williams L, Maier M, Dunstan R, Salloway S, Chen T, Ling Y, et al. The antibody aducanumab reduces Abeta plaques in Alzheimer's disease. Nature. 2016;537:50–6.
87. Sperling R, Salloway S, Brooks DJ, Tampieri D, Barakos J, Fox NC, Raskind M, Sabbagh M, Honig LS, Porsteinsson AP, et al. Amyloid-related imaging abnormalities in patients with Alzheimer's disease treated with bapineuzumab: a retrospective analysis. Lancet Neurol. 2012;11:241–9.
88. Sperling RA, Jack CR Jr, Black SE, Frosch MP, Greenberg SM, Hyman BT, Scheltens P, Carrillo MC, Thies W, Bednar MM, et al. Amyloid-related imaging abnormalities in amyloid-modifying therapeutic trials: recommendations from the Alzheimer's Association Research Roundtable Workgroup. Alzheimer's Dementia. 2011;7:367–85.
89. Taylor X, Clark IM, Fitzgerald GJ, Oluoch H, Hole JT, DeMattos RB, Wang Y, Pan F. Amyloid-beta (Abeta) immunotherapy induced microhemorrhages are associated with activated perivascular macrophages and peripheral monocyte recruitment in Alzheimer's disease mice. Mol Neurodegener. 2023;18:59.
90. Castellani RJ, Shanes ED, McCord M, Reish NJ, Flanagan ME, Mesulam MM, Jamshidi P. Neuropathology of Anti-Amyloid-beta Immunotherapy: A Case Report. J Alzheimers Dis. 2023;93:803–13.
91. Huang W, Li R, Zhang J, Cheng Y, Ramakrishnan DP, Silverstein RL. A CD36 transmembrane domain peptide interrupts CD36 interactions with membrane partners on macrophages and inhibits atherogenic functions. Transl Res. 2023;254:68–76.
92. Wang L, Bao Y, Yang Y, Wu Y, Chen X, Si S, Hong B. Discovery of antagonists for human scavenger receptor CD36 via an ELISA-like high-throughput screening assay. J Biomol Screen. 2010;15:239–50.
93. Wilkinson K, Boyd JD, Glicksman M, Moore KJ, El Khoury J. A high content drug screen identifies ursolic acid as an inhibitor of amyloid beta protein interactions with its receptor CD36. J Biol Chem. 2011;286:34914–22.
94. Zhou L, Li HY, Wang JH, Deng ZZ, Shan YL, Tan S, Shi YH, Zhang MX, Liu SX, Zhang BJ, et al. Correlation of gene polymorphisms of CD36 and ApoE with susceptibility of Alzheimer disease: A case-control study. Medicine (Baltimore). 2018;97:e12470.
95. Sery O, Zeman T, Sheardova K, Vyhnalek M, Markova H, Laczo J, Lochman J, Kralik P, Vrzalova K, Dziedzinska R, et al. Six genetically linked mutations in the CD36 gene significantly delay the onset of Alzheimer's disease. Sci Rep. 2022;12:10994.
96. Larochelle A, Bellavance MA, Michaud JP, Rivest S. Bone marrow-derived macrophages and the CNS: An update on the use of experimental chimeric mouse models and bone marrow transplantation in neurological disorders. Biochim Biophys Acta. 2016;1862:310–22.
97. Diserbo M, Agin A, Lamproglou I, Mauris J, Staali F, Multon E, Amourette C. Blood-brain barrier permeability after gamma whole-body irradiation: an in vivo microdialysis study. Can J Physiol Pharmacol. 2002;80:670–8.
98. Amann L, Masuda T, Prinz M: Mechanisms of myeloid cell entry to the healthy and diseased central nervous system. Nat Immunol 2023.

99. Thal DR, Ghebremedhin E, Rub U, Yamaguchi H, Del Tredici K, Braak H. Two types of sporadic cerebral amyloid angiopathy. J Neuropathol Exp Neurol. 2002;61:282–93.
100. Weller RO. Pathology of cerebrospinal fluid and interstitial fluid of the CNS: significance for Alzheimer disease, prion disorders and multiple sclerosis. J Neuropathol Exp Neurol. 1998;57:885–94.
101. Roher AE, Kuo YM, Esh C, Knebel C, Weiss N, Kalback W, Luehrs DC, Childress JL, Beach TG, Weller RO, Kokjohn TA. Cortical and leptomeningeal cerebrovascular amyloid and white matter pathology in Alzheimer's disease. Mol Med. 2003;9:112–22.
102. Koemans EA, Chhatwal JP, van Veluw SJ, van Etten ES, van Osch MJP, van Walderveen MAA, Sohrabi HR, Kozberg MG, Shirzadi Z, Terwindt GM, et al. Progression of cerebral amyloid angiopathy: a pathophysiological framework. Lancet Neurol. 2023;22:632–42.
103. Jaunmuktane Z, Mead S, Ellis M, Wadsworth JD, Nicoll AJ, Kenny J, Launchbury F, Linehan J, Richard-Loendt A, Walker AS, et al. Evidence for human transmission of amyloid-beta pathology and cerebral amyloid angiopathy. Nature. 2015;525:247–50.

Publisher's Note